Composites: Part B 43 (2012) 2577–2593

Contents lists available at SciVerse ScienceDirect

Composites: Part B

journal homepage: www.elsevier.com/locate/compositesb

Effective mechanical properties of "fuzzy fiber" composites

George Chatzigeorgiou [a], Gary Don Seidel [b], Dimitris C. Lagoudas [c,*]

[a] Dept. of Civil Engineering, Aristotle University of Thessaloniki, Thessaloniki 54124, Greece
[b] Dept. of Aerospace and Ocean Engineering, Virginia Polytechnic Institute and State University, 228 Randolph Hall (0203), Blacksburg, VA 24061, USA
[c] Dept. of Aerospace Engineering, Texas A&M University, College Station, TX 77843, USA

ARTICLE INFO

Article history:
Received 29 November 2011
Received in revised form 19 February 2012
Accepted 4 March 2012
Available online 16 March 2012

Keywords:
A. Carbon fibre
A. Polymer–matrix composites
C. Micro-mechanics
Carbon nanotubes

ABSTRACT

In this paper we investigate the mechanical behavior of carbon fiber composites, where the carbon fibers are coated with radially aligned carbon nanotubes. For this purpose we develop a general micromechanics method for fiber composites, where fibers are coated with radially aligned microfibers ("fuzzy fiber" composites). The mechanical effective properties are computed with a special extension of the composite cylinders method. The in-plane shear modulus is determined using an extended version of the Christensen's generalized self consistent composite cylinders method. The proposed methodology provides stress and strain concentration tensors. The results of the method are compared with numerical approaches based on the asymptotic expansion homogenization method. The combination of composite cylinders method and Mori–Tanaka method allows us to compute effective properties of composites with multiple types of "fuzzy fibers". Numerical examples of composites made of epoxy resin, carbon fibers and carbon nanotubes are presented and the impact of the carbon nanotubes length and volume fraction in the overall composite properties is studied.

1. Introduction

Since the discovery of carbon nanotubes (CNTs) by Iijima [24], there has been a significant research effort directed towards understanding the source of their exceptional properties and how to take advantage of those properties in the design of macroscale nanocomposites. A single-walled carbon nanotube can be viewed as a single sheet of graphite (i.e., graphene), which has been rolled into the shape of a tube [43]. Single walled CNTs have radii on the order of nanometers and lengths on the order of micrometers resulting in large aspect ratios beneficial to their use in composites [43,40]. Carbon nanotubes are reported to have an axial Young's modulus in the range of 300–1000 GPa, up to five times the stiffness and with half the density of SiC fibers, in addition to having a theoretically predicted elongation to break of 30–40% [58,59,61,57,44,13,36].

A wide variety of composites containing CNTs have been manufactured [31,35,37] Polymer-wrapped and functionalized CNTs, producing distinct interphase regions between matrix and CNTs, are also well documented in the literature [56,28,49,30,63]. Recent efforts focus on using CNTs in order to enhance the properties of microscale fiber composites. In order to strengthen the interface between the fiber and the matrix, the fibers can be coated with CNTs before being embedded in the matrix. This technique has been developed for carbon fibers [52,29,42,64,62], ceramic fibers [60,9] and glass fibers [2].

Modeling of composites containing CNTs has also received attention in recent years. Frankland et al. [16] have used molecular dynamics to obtain the stress–strain behavior of CNTs embedded in a polymer matrix. Liu and Chen [27] studied the mechanical response in tension of a single CNT embedded in polymer via finite element analysis. Odegard et al. [34] have modeled CNT composites using the equivalent continuum method in conjunction with the Mori–Tanaka micromechanics method to obtain the effective elastic constants for both aligned and misaligned CNTs. Spanos and Kontsos [48] have used Monte Carlo finite element method in order to obtain nanocomposite properties. The effects of nanotube waviness on the effective composite properties have been studied by Fisher et al. [13,14] using finite element analysis in conjunction with the Mori–Tanaka method. Buckling of CNTs within an epoxy matrix has been considered by Hadjiev et al. [18]. Other efforts have focused on the inclusion of less than ideal CNT adhesion to the matrix in CNT composite modeling [55,15,17]. The clustering of CNTs in the polymer matrix was studied in Seidel and Lagoudas [47]. In all these modeling efforts the composite consists of carbon nanotubes and matrix.

Herein we examine composites where carbon fibers, coated with radially aligned carbon nanotubes, are embedded in a matrix. These enhanced carbon fibers have the potential to improve not only interface strength, but to provide additional functionality as sensors by taking advantage of the multifunctional properties of

* Corresponding author.
E-mail address: lagoudas@tamu.edu (D.C. Lagoudas).

1359-8368/$ - see front matter © 2012 Published by Elsevier Ltd.
http://dx.doi.org/10.1016/j.compositesb.2012.03.001

Report Documentation Page

Form Approved
OMB No. 0704-0188

1. REPORT DATE	2. REPORT TYPE	3. DATES COVERED
2012		**00-00-2012 to 00-00-2012**

4. TITLE AND SUBTITLE	5a. CONTRACT NUMBER
Effective mechanical properties of 'fuzzy fiber' composites	5b. GRANT NUMBER
	5c. PROGRAM ELEMENT NUMBER
6. AUTHOR(S)	5d. PROJECT NUMBER
	5e. TASK NUMBER
	5f. WORK UNIT NUMBER
7. PERFORMING ORGANIZATION NAME(S) AND ADDRESS(ES) **Texas A&M University,Department of Aerospace Engineering,College Station,TX,77843**	8. PERFORMING ORGANIZATION REPORT NUMBER
9. SPONSORING/MONITORING AGENCY NAME(S) AND ADDRESS(ES)	10. SPONSOR/MONITOR'S ACRONYM(S)
	11. SPONSOR/MONITOR'S REPORT NUMBER(S)

12. DISTRIBUTION/AVAILABILITY STATEMENT
Approved for public release; distribution unlimited

13. SUPPLEMENTARY NOTES

14. ABSTRACT

In this paperweinvestigate the mechanical behavior of carbon fiber composites, where the carbon fibers are coated with radially aligned carbon nanotubes. For this purpose we develop a general micromechanics method for fiber composites, where fibers are coated with radially aligned microfibers (??fuzzy fiber?? composites). The mechanical effective properties are computed with a special extension of the composite cylinders method. The in-plane shear modulus is determined using an extended version of the Christensen?s generalized self consistent composite cylinders method. The proposed methodology provides stress and strain concentration tensors. The results of the method are compared with numerical approaches based on the asymptotic expansion homogenization method. The combination of composite cylinders method and Mori?Tanaka method allows us to compute effective properties of composites with multiple types of ??fuzzy fibers??. Numerical examples of composites made of epoxy resin, carbon fibers and carbon nanotubes are presented and the impact of the carbon nanotubes length and volume fraction in the overall composite properties is studied.

15. SUBJECT TERMS

16. SECURITY CLASSIFICATION OF:			17. LIMITATION OF ABSTRACT	18. NUMBER OF PAGES	19a. NAME OF RESPONSIBLE PERSON
a. REPORT **unclassified**	b. ABSTRACT **unclassified**	c. THIS PAGE **unclassified**	**Same as Report (SAR)**	**17**	

CNTs. In the literature there are several models, which attempt to identify the overall behavior of such composites. Kundalwal and Ray [26] identify the mechanical response of fuzzy fiber composites using the method of materials approach, while Chatzigeorgiou et al. [5] compute numerically the effective mechanical properties through the asymptotic expansion homogenization method. Ray [39] introduces a shear lag model for obtaining the behavior of composites reinforced with carbon nanotubes-coated piezoelectric fibers.

In the present work we investigate the effective properties of fiber composites, where the fibers are coated with radially aligned microfibers ("fuzzy fibers"). In order to achieve this goal, we use the generalized self consistent composite cylinders method [20,7,47], modified properly in order to account for the additional interface layer between the fiber and the matrix. The proposed methodology is utilized in numerical examples, in which carbon fibers, coated with radially aligned carbon nanotubes, are embedded in an epoxy matrix.

The structure of this paper is the following: in Section 2 we describe the characteristics of the "fuzzy fiber" composite and we present the major model assumptions. Section 3 presents the modified generalized self consistent composite cylinders method. In Section 4 we discuss how the method can be applied in the case of mixed type "fuzzy fiber" composites, while Section 5 shows some numerical examples. The conclusions of this work are summarized in the final section.

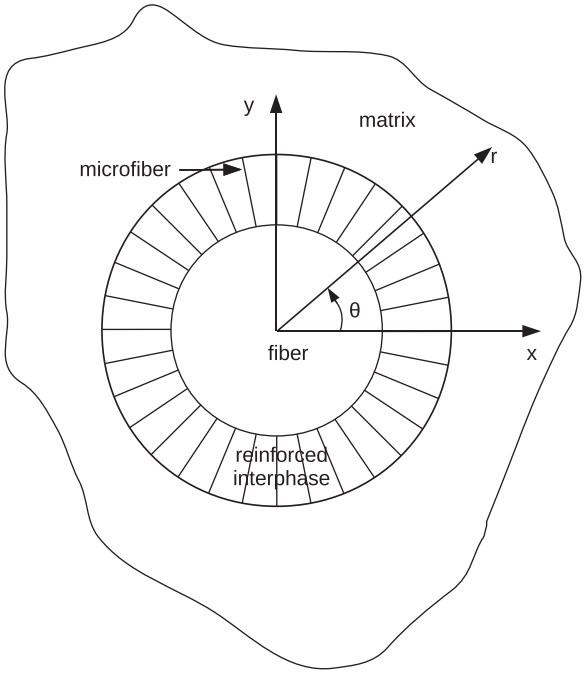

Fig. 2. RVE of the "fuzzy fiber" material system.

2. "Fuzzy fiber" composites

The "fuzzy fiber" material system is a fiber composite (Fig. 1a), in which the fibers are coated with radially aligned microfibers (Fig. 1b). For modeling purposes we assume that the representative volume element (RVE) of the "fuzzy fiber" composite contains three layers: the first layer is the cylindrical fiber. The second is a reinforced interphase (intermediate cylindrical layer) which consists of cylindrical microfibers and matrix. The third layer is the area of the pure matrix (Fig. 2). The coated fibers are arranged to correspond to a unidirectional lamina layer, in which the fibers are aligned in the z-direction and are well dispersed (randomly distributed) in the x–y plane (Fig. 1a). The fibers are made by isotropic, or transversely isotropic linearly elastic material with the axis of symmetry parallel to the axis of the fibers, while the material of the matrix is assumed isotropic. The microfibers in the reinforced interphase are assumed to be transversely isotropic with the axis of symmetry parallel with the microfibers axis (r direction in Fig. 1b). The idealized RVE of the reinforced interphase is shown in Fig. 3. Based on the observations that (a) the diameter of the fiber is very large compared to the diameter of the microfibers and (b) the microfibers are normally densely packed along the fiber interpase (small $\Delta\theta$ in Fig. 3), we can assume that the reinforced interphase behaves as a classical unidirectional composite, and effectively it is a transversely isotropic medium with the axis of symmetry parallel to the axis of microfibers (i.e. in the radial direction of the fiber). Hence, we can use micromechanics methods for composites with aligned microfibers in determining the transversely isotropic interphase properties [47]. In Kundalwal and Ray [26] the properties of the reinforced interphase are represented in Cartesian coordinate system (see Appendix A) and the effective behavior is assumed to be given by averaging over all orientations. Such an approach leads to alter the anisotropic nature of the reinforced interphase, which is identified as transversely isotropic material with axis of symmetry

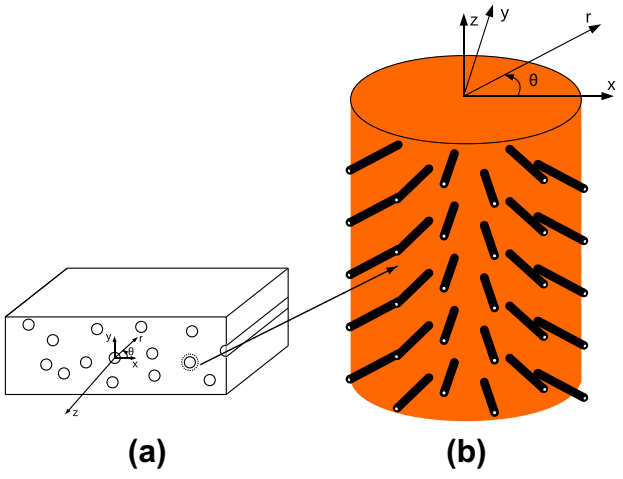

Fig. 1. Schematic of (a) the "fuzzy fiber" lamina layer and (b) the "fuzzy fiber".

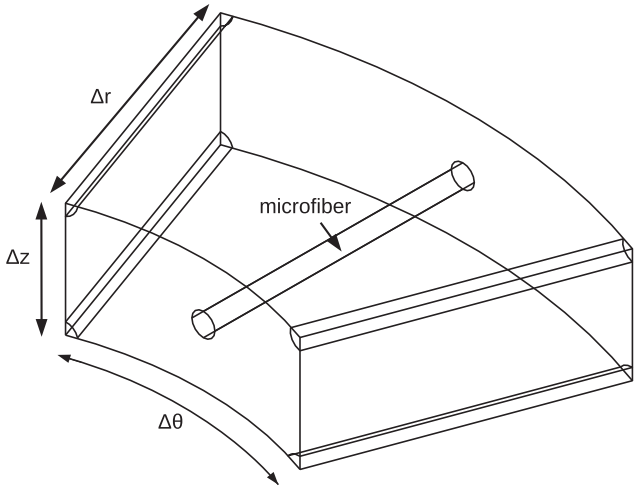

Fig. 3. RVE of the reinforced interphase.

parallel to the axis of the fiber (not the microfiber). The methodology we propose in this work avoids such an assumption.

In the cylindrical coordinate system shown in Figs. 1b and 2, where z is the fiber longitudinal axis, the stress–strain relations of the matrix, the fiber and the intermediate layer (reinforced interphase) are written

$$\begin{pmatrix}\sigma^m_{rr}\\ \sigma^m_{\theta\theta}\\ \sigma^m_{zz}\\ \sigma^m_{z\theta}\\ \sigma^m_{rz}\\ \sigma^m_{r\theta}\end{pmatrix}=\begin{pmatrix} C^m_{11} & C^m_{12} & C^m_{12} & 0 & 0 & 0\\ C^m_{12} & C^m_{11} & C^m_{12} & 0 & 0 & 0\\ C^m_{12} & C^m_{12} & C^m_{11} & 0 & 0 & 0\\ 0 & 0 & 0 & \frac{C^m_{11}-C^m_{12}}{2} & 0 & 0\\ 0 & 0 & 0 & 0 & \frac{C^m_{11}-C^m_{12}}{2} & 0\\ 0 & 0 & 0 & 0 & & \frac{C^m_{11}-C^m_{12}}{2}\end{pmatrix}\begin{pmatrix}\varepsilon^m_{rr}\\ \varepsilon^m_{\theta\theta}\\ \varepsilon^m_{zz}\\ 2\varepsilon^m_{z\theta}\\ 2\varepsilon^m_{rz}\\ 2\varepsilon^m_{r\theta}\end{pmatrix}, \tag{1}$$

$$\begin{pmatrix}\sigma^f_{rr}\\ \sigma^f_{\theta\theta}\\ \sigma^f_{zz}\\ \sigma^f_{z\theta}\\ \sigma^f_{rz}\\ \sigma^f_{r\theta}\end{pmatrix}=\begin{pmatrix} C^f_{11} & C^f_{12} & C^f_{13} & 0 & 0 & 0\\ C^f_{12} & C^f_{11} & C^f_{13} & 0 & 0 & 0\\ C^f_{13} & C^f_{13} & C^f_{33} & 0 & 0 & 0\\ 0 & 0 & 0 & C^f_{44} & 0 & 0\\ 0 & 0 & 0 & 0 & C^f_{44} & 0\\ 0 & 0 & 0 & 0 & & \frac{C^f_{11}-C^f_{12}}{2}\end{pmatrix}\begin{pmatrix}\varepsilon^f_{rr}\\ \varepsilon^f_{\theta\theta}\\ \varepsilon^f_{zz}\\ 2\varepsilon^f_{z\theta}\\ 2\varepsilon^f_{rz}\\ 2\varepsilon^f_{r\theta}\end{pmatrix}, \tag{2}$$

$$\begin{pmatrix}\sigma^{int}_{rr}\\ \sigma^{int}_{\theta\theta}\\ \sigma^{int}_{zz}\\ \sigma^{int}_{z\theta}\\ \sigma^{int}_{rz}\\ \sigma^{int}_{r\theta}\end{pmatrix}=\begin{pmatrix} C^{int}_{11} & C^{int}_{12} & C^{int}_{12} & 0 & 0 & 0\\ C^{int}_{12} & C^{int}_{22} & C^{int}_{23} & 0 & 0 & 0\\ C^{int}_{12} & C^{int}_{23} & C^{int}_{22} & 0 & 0 & 0\\ 0 & 0 & 0 & \frac{C^{int}_{22}-C^{int}_{23}}{2} & 0 & 0\\ 0 & 0 & 0 & 0 & C^{int}_{66} & 0\\ 0 & 0 & 0 & 0 & & C^{int}_{66}\end{pmatrix}\begin{pmatrix}\varepsilon^{int}_{rr}\\ \varepsilon^{int}_{\theta\theta}\\ \varepsilon^{int}_{zz}\\ 2\varepsilon^{int}_{z\theta}\\ 2\varepsilon^{int}_{rz}\\ 2\varepsilon^{int}_{r\theta}\end{pmatrix}, \tag{3}$$

where the indices 1, 2, 3 in the stiffness tensors denote the axes r, θ, z respectively. In the case of the unidirectional "fuzzy fiber" composite, absence of the reinforced interphase (i.e. just fiber in matrix lamina) leads to transversely isotropic effective medium. Moreover we can easily show that, upon arbitrary rotation about the z axis, the stiffness matrix of the reinforced interphase remains the same (see Appendix A), which indicates that the quasi-cylindrically orthotropic structure (transversely isotropic with axis of symmetry parallel to the direction r of Fig. 2) of the reinforced interphase does not disrupt the overall symmetry of the effective medium. This means that the final composite material will be effectively transversely isotropic, with the axis of symmetry parallel to the axis of the fibers (the z axis). As such, the stress–strain relation of the effective unidirectional lamina in the cylindrical coordinate system is given by

$$\begin{pmatrix}\sigma^{\text{eff}}_{rr}\\ \sigma^{\text{eff}}_{\theta\theta}\\ \sigma^{\text{eff}}_{zz}\\ \sigma^{\text{eff}}_{z\theta}\\ \sigma^{\text{eff}}_{rz}\\ \sigma^{\text{eff}}_{r\theta}\end{pmatrix}=\begin{pmatrix} C^{\text{eff}}_{11} & C^{\text{eff}}_{12} & C^{\text{eff}}_{13} & 0 & 0 & 0\\ C^{\text{eff}}_{12} & C^{\text{eff}}_{11} & C^{\text{eff}}_{13} & 0 & 0 & 0\\ C^{\text{eff}}_{13} & C^{\text{eff}}_{13} & C^{\text{eff}}_{33} & 0 & 0 & 0\\ 0 & 0 & 0 & C^{\text{eff}}_{44} & 0 & 0\\ 0 & 0 & 0 & 0 & C^{\text{eff}}_{44} & 0\\ 0 & 0 & 0 & 0 & & \frac{C^{\text{eff}}_{11}-C^{\text{eff}}_{12}}{2}\end{pmatrix}\begin{pmatrix}\varepsilon^{\text{eff}}_{rr}\\ \varepsilon^{\text{eff}}_{\theta\theta}\\ \varepsilon^{\text{eff}}_{zz}\\ 2\varepsilon^{\text{eff}}_{z\theta}\\ 2\varepsilon^{\text{eff}}_{rz}\\ 2\varepsilon^{\text{eff}}_{r\theta}\end{pmatrix}. \tag{4}$$

The computation of the effective properties requires knowledge of the mechanical response of the "fuzzy fiber" material system, which ideally consists of concentric cylinders (Fig. 4). The elastic response of homogeneous and non-homogeneous thick- or thin-walled tubes under different boundary conditions was studied by Chatterjee [3], Horg and Chan [21,22], Chen et al. [6], Tarn and Wang [51], Tarn [50], Ruhi et al. [41], Hosseini Kordkheili and Naghdabadi [23], Chatzigeorgiou et al. [4], Tsukrov and Drach [53], Nie and Batra [32,33]. Our aim is to determine elasticity solutions for a series of boundary value problems (BVPs). These BVPs are used in conjunction with the composite cylinders method in order to identify the effective properties of the composite, as has been successfully implemented in the past in the case of CNT composites [47].

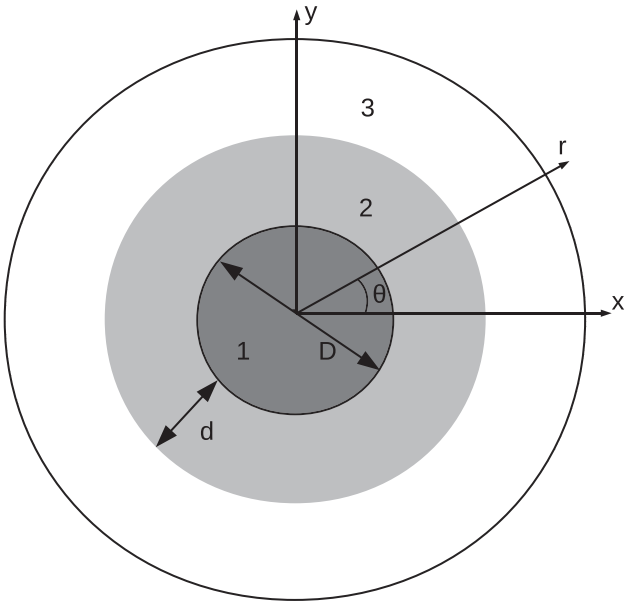

Fig. 4. RVE of the composite material for the composite cylinders method.

3. Composite cylinders method

For the composite cylinders method we use the RVE of Fig. 4. This 3 layer composite cylinder RVE (fiber, reinforced interphase, matrix) is equivalent with an RVE for a randomly distributed, aligned, "fuzzy fiber" composite (additional details are given in [20,7,47]. The proposed approach can be extended for cases where the number of layers are $N \geqslant 3$.

It the following, we will consider the cylindrical as the global coordinate system. In cylindrical coordinates the equilibrium equations are given by

$$\frac{\partial\sigma^{(i)}_{rr}}{\partial r}+\frac{1}{r}\frac{\partial\sigma^{(i)}_{r\theta}}{\partial\theta}+\frac{\sigma^{(i)}_{rr}-\sigma^{(i)}_{\theta\theta}}{r}+\frac{\partial\sigma^{(i)}_{rz}}{\partial z}=0, \tag{5}$$

$$\frac{\partial\sigma^{(i)}_{r\theta}}{\partial r}+\frac{1}{r}\frac{\partial\sigma^{(i)}_{\theta\theta}}{\partial\theta}+2\frac{\sigma^{(i)}_{r\theta}}{r}+\frac{\partial\sigma^{(i)}_{z\theta}}{\partial z}=0, \tag{6}$$

$$\frac{\partial\sigma^{(i)}_{rz}}{\partial r}+\frac{1}{r}\frac{\partial\sigma^{(i)}_{z\theta}}{\partial\theta}+\frac{\sigma^{(i)}_{rz}}{r}+\frac{\partial\sigma^{(i)}_{zz}}{\partial z}=0, \tag{7}$$

where (i) is the material layer ($i = 1,2,\ldots,N$). Assuming small deformation gradients, the infinitesimal strains are expressed with respect to the displacements according to the relations

$$\begin{aligned}&\varepsilon^{(i)}_{rr}=\frac{\partial u^{(i)}_r}{\partial r},\quad \varepsilon^{(i)}_{\theta\theta}=\frac{1}{r}\left(\frac{\partial u^{(i)}_\theta}{\partial\theta}+u^{(i)}_r\right),\quad \varepsilon^{(i)}_{zz}=\frac{\partial u^{(i)}_z}{\partial z},\\ &2\varepsilon^{(i)}_{z\theta}=\frac{\partial u^{(i)}_\theta}{\partial z}+\frac{1}{r}\frac{\partial u^{(i)}_z}{\partial\theta},\quad 2\varepsilon^{(i)}_{rz}=\frac{\partial u^{(i)}_z}{\partial r}+\frac{\partial u^{(i)}_r}{\partial z},\\ &2\varepsilon^{(i)}_{r\theta}=\frac{1}{r}\frac{\partial u^{(i)}_r}{\partial\theta}+\frac{\partial u^{(i)}_\theta}{\partial r}-\frac{u^{(i)}_\theta}{r}.\end{aligned} \tag{8}$$

In order to use the composite cylinders method, we need to determine admissible displacement fields which will satisfy five specific boundary value problems. In order to do this, we have to

substitute (8) into the appropriate constitutive relations (1)–(3), and then substitute the resulting equations into (5)–(7) to get the equilibrium equations in terms of the displacements. Next we can apply the semi-inverse method to determine the necessary admissible displacement fields. Then, solving the same boundary value problems for the homogenized cylinder we can obtain the effective properties using the direct strain energy equivalency method. The homogenized cylinder is described by the same equations, with the difference that the (i) must be replaced by eff denoting the effective material. Tsukrov and Drach [54] present a similar approach with the above described, for the case of carbon/carbon composites, where pyrolytic carbon cylindrically orthotropic layers surround a fiber. In their study they obtain the effective axial Young's modulus, the transverse bulk modulus and the axial Poisson's ratio. The admissible displacement fields they used are presented in Tsukrov and Drach [53]. In the present work we obtain five effective properties (in-plane bulk modulus, axial shear modulus, axial Young's modulus, axial stiffness coefficient, in-plane shear modulus) which are sufficient to describe the overall behavior of the "fuzzy fiber" composite. The in-plane shear modulus requires special treatment, since the composite cylinders method provide only bounds. For this material property we need to use the generalized self consistent composite cylinders method proposed by Christensen [7].

In the following, we denote r_i to be the external radius of each layer, with the inner radius of the solid fiber layer denoted $r_0 = 0$. The length of the composite cylinder is taken as $2L$. We also introduce the volume average

$$\langle \phi \rangle = \frac{1}{V}\int_V \phi(x,y,z)dx\,dy\,dz = \frac{1}{V}\int_V r\phi(r,\theta,z)dr\,d\theta\,dz, \tag{9}$$

where V is the volume of the RVE.

3.1. In-plane bulk modulus

The in-plane, or plane strain bulk modulus, K_{12}^{eff}, is determined through the application of the displacement field

$$u_r^{(i)} = \sum_{j=1}^{2} D_j^{(i)} r^{n_j^{(i)}}, \quad u_\theta^{(i)} = u_z^{(i)} = 0, \;\; i = 1,\ldots,N, \tag{10}$$

with

$$n_1^{(i)} = \sqrt{C_{22}^{(i)}/C_{11}^{(i)}} = -n_2^{(i)}. \tag{11}$$

For isotropic and transversely isotropic materials with axis of symmetry parallel to the axis of the fiber $n_1^{(i)} = -n_2^{(i)} = 1$ and the displacement field reduces to the expression described in Seidel and Lagoudas [47]. $D_1^{(i)}$ and $D_2^{(i)}$ are constants which are determined from the boundary condition (Fig. 5a)

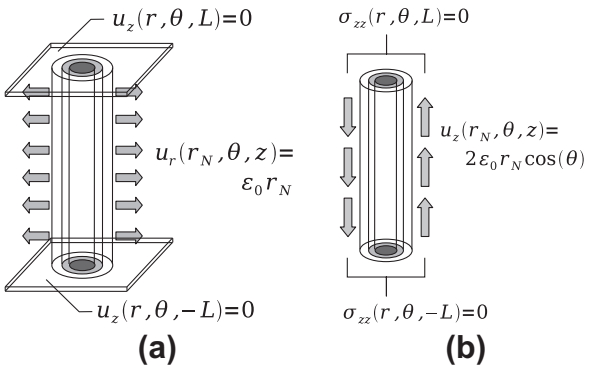

Fig. 5. BVP for (a) in-plane bulk modulus and (b) axial shear modulus.

$$u_r^{(N)}(r_N) = \varepsilon_0 r_N, \tag{12}$$

the condition

$$D_2^{(1)} = 0, \tag{13}$$

which insures that the displacements remain bounded at the origin, and the continuity conditions

$$u_r^{(i)}(r_i) = u_r^{(i+1)}(r_i), \;\; \sigma_{rr}^{(i)}(r_i) = \sigma_{rr}^{(i+1)}(r_i), \;\; \text{for } i = 1,\ldots,N-1, \tag{14}$$

which enforces perfect bonding between phase layers. The volume averaged strain energy for the composite cylinder assemblage is given by

$$\begin{aligned} W^{\text{RVE}} &= \frac{1}{2}\left\langle \sigma_{rr}^{(i)}\varepsilon_{rr}^{(i)} + \sigma_{\theta\theta}^{(i)}\varepsilon_{\theta\theta}^{(i)} \right\rangle \\ &= \frac{1}{r_N^2}\sum_{i=1}^{N}\sum_{j=1}^{2}\left(\frac{C_{22}^{(i)}}{n_j^{(i)}} + C_{12}^{(i)}\right)\left(D_j^{(i)}\right)^2\left(r_i^{2n_j^{(i)}} - r_{i-1}^{2n_j^{(i)}}\right). \end{aligned} \tag{15}$$

The homogenized cylinder is described by the same equations, with the difference that the (i) must be replaced by eff and $n_{\text{eff}} = 1$. For the effective medium we get $D_1^{\text{eff}} = \varepsilon_0$. Consequently the strain energy of the effective homogeneous material is written as

$$W^{\text{eff}} = \frac{1}{2}\left\langle \sigma_{rr}^{\text{eff}}\varepsilon_{rr}^{\text{eff}} + \sigma_{\theta\theta}^{\text{eff}}\varepsilon_{\theta\theta}^{\text{eff}} \right\rangle = 2K_{12}^{\text{eff}}\varepsilon_0^2. \tag{16}$$

Since $W^{\text{RVE}} = W^{\text{eff}}$, we get

$$K_{12}^{\text{eff}} = \frac{1}{2\varepsilon_0^2 r_N^2}\sum_{i=1}^{N}\sum_{j=1}^{2}\left(\frac{C_{22}^{(i)}}{n_j^{(i)}} + C_{12}^{(i)}\right)\left(D_j^{(i)}\right)^2\left(r_i^{2n_j^{(i)}} - r_{i-1}^{2n_j^{(i)}}\right). \tag{17}$$

Here we need to mention that the effective in-plane bulk modulus does not depend on the applied strain at the boundary as it can be shown that $D_j^{(i)}$ contains ε_0.

3.2. Axial shear modulus

The axial shear modulus, $\mu_{23}^{\text{eff}} = C_{44}^{\text{eff}}$, is determined through the application of the displacement field

$$u_z^{(i)} = \sum_{j=1}^{2} D_j^{(i)} r^{n_j^{(i)}}\cos\theta, u_\theta^{(i)} = u_r^{(i)} = 0, \tag{18}$$

with

$$n_1^{(i)} = \sqrt{C_{44}^{(i)}/C_{55}^{(i)}} = -n_2^{(i)}. \tag{19}$$

For isotropic and transversely isotropic materials with axis of symmetry parallel to the axis of the fiber $n_1^{(i)} = -n_2^{(i)} = 1$ and the displacement field reduces to the expression described in Seidel and Lagoudas [47]. $D_1^{(i)}$ and $D_2^{(i)}$ are constants which are determined from the boundary condition (Fig. 5b)

$$u_z^{(N)}(r_N,\theta) = 2\varepsilon_0 r_N\cos\theta, \tag{20}$$

the condition for bounded displacements at the origin

$$D_2^{(1)} = 0, \tag{21}$$

and the continuity conditions

$$\begin{aligned} &u_z^{(i)}(r_i,\theta) = u_z^{(i+1)}(r_i,\theta), \sigma_{rz}^{(i)}(r_i,\theta) = \sigma_{rz}^{(i+1)}(r_i,\theta), \\ &\quad \text{for } i = 1,\ldots,N-1. \end{aligned} \tag{22}$$

The volume averaged strain energy of the composite is given by

$$\begin{aligned} W^{\text{RVE}} &= \frac{1}{2}\left\langle 2\sigma_{z\theta}^{(i)}\varepsilon_{z\theta}^{(i)} + 2\sigma_{rz}^{(i)}\varepsilon_{rz}^{(i)} \right\rangle \\ &= \frac{1}{2r_N^2}\sum_{i=1}^{N}\sum_{j=1}^{2}\frac{C_{44}^{(i)}}{n_j^{(i)}}\left(D_j^{(i)}\right)^2\left(r_i^{2n_j^{(i)}} - r_{i-1}^{2n_j^{(i)}}\right). \end{aligned} \tag{23}$$

The homogenized cylinder is described by the same equations, with the difference that the (i) must be replaced by eff and $n_{\text{eff}} = 1$. For the effective medium we get $D_1^{\text{eff}} = 2\varepsilon_0$ and

$$W^{\text{eff}} = \frac{1}{2}\left\langle 2\sigma_{z\theta}^{\text{eff}}\varepsilon_{z\theta}^{\text{eff}} + 2\sigma_{rz}^{\text{eff}}\varepsilon_{rz}^{\text{eff}}\right\rangle = 2\mu_{23}^{\text{eff}}\varepsilon_0^2. \tag{24}$$

Since $W^{\text{RVE}} = W^{\text{eff}}$, we get

$$\mu_{23}^{\text{eff}} = \frac{1}{4\varepsilon_0^2 r_N^2}\sum_{i=1}^{N}\sum_{j=1}^{2}\frac{C_{44}^{(i)}}{n_j^{(i)}}\left(D_j^{(i)}\right)^2\left(r_i^{2n_j^{(i)}} - r_{i-1}^{2n_j^{(i)}}\right). \tag{25}$$

3.3. Axial Young's modulus and axial stiffness component

The axial Young's modulus, E_3^{eff} and the axial stiffness component, C_{33}^{eff}, are determined through the application of the displacement field

$$u_r^{(j)} = \Lambda^{(i)} r + \sum_{j=1}^{2} D_j^{(i)} r^{n_j^{(i)}}, \quad \Lambda^{(i)} = \begin{cases} \frac{C_{13}^{(i)} - C_{23}^{(i)}}{C_{22}^{(i)} - C_{11}^{(i)}}\varepsilon_0, & C_{11}^{(i)} \neq C_{22}^{(i)}, \\ 0, & C_{11}^{(i)} = C_{22}^{(i)}, \end{cases} \tag{26}$$

$$u_\theta^{(i)} = 0, \quad u_z^{(i)} = \varepsilon_0 z, \quad \text{for } i = 1, \ldots, N,$$

with

$$n_1^{(i)} = \sqrt{C_{22}^{(i)}/C_{11}^{(i)}} = -n_2^{(i)}. \tag{27}$$

For isotropic and transversely isotropic materials with axis of symmetry parallel to the axis of the fiber $n_1^{(i)} = 1$. Relative to an isotropic or transversely isotropic interphase with aligned symmetry axis with the overall symmetry axis [47], the reinforced interphase behavior introduces a new term, $\Lambda^{(i)} r$, which is needed to satisfy the equilibrium Eq. (5). $\Lambda^{(i)}$ takes a non-zero value only in the case where the material has different radial and circumferential behavior. It also carries the ε_0 from the boundary condition (Fig. 6) which permeates into the solution of the form for $u_r^{(j)}$. The constants $D_1^{(i)}$ and $D_2^{(i)}$, $i = 1, \ldots, N$ are determined from the continuity conditions

$$u_r^{(i)}(r_i) = u_r^{(i+1)}(r_i), \quad \sigma_{rr}^{(i)}(r_i) = \sigma_{rr}^{(i+1)}(r_i), \quad \text{for } i = 1, \ldots, N-1. \tag{28}$$

the condition for bounded displacement at the origin

$$D_2^{(1)} = 0, \tag{29}$$

and the boundary conditions. The displacement u_z is also trivially enforced. For the axial Young's modulus, the lateral surface is traction free in the tension test

$$\sigma_{rr}^{(N)}(r_N) = 0, \tag{30}$$

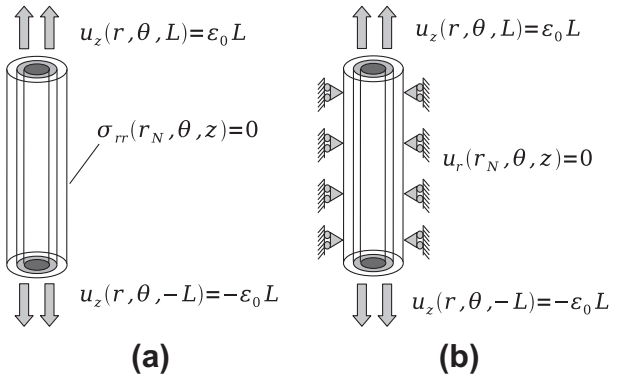

Fig. 6. BVP for (a) axial Young's modulus and (b) axial stiffness coefficient.

while for the axial stiffness component the lateral surface is constrained in the stiffness test

$$u_r^{(N)}(r_N) = 0. \tag{31}$$

For the composite we have

$$\begin{aligned} W^{\text{RVE}} &= \frac{1}{2}\left\langle \sigma_{rr}^{(i)}\varepsilon_{rr}^{(i)} + \sigma_{\theta\theta}^{(i)}\varepsilon_{\theta\theta}^{(i)} + \sigma_{zz}^{(i)}\varepsilon_{zz}^{(i)}\right\rangle \\ &= \frac{1}{r_N^2}\sum_{i=1}^{N}\left[\left(\Lambda_1^{(i)}\varepsilon_0 + 2\Lambda_2^{(i)}\Lambda^{(i)}\right)\frac{r_i^2 - r_{i-1}^2}{2} + 2\varepsilon_0\sum_{j=1}^{2}D_j^{(i)}\left(C_{23}^{(i)} + n_j^{(i)}C_{13}^{(i)}\right)\right. \\ &\quad \times K_j^{(i)} + \sum_{j=1}^{2}\left(\frac{C_{22}^{(i)}}{n_j^{(i)}} + C_{12}^{(i)}\right)D_j^{(i)}\left(D_j^{(i)}\left(r_i^{2n_j^{(i)}} - r_{i-1}^{2n_j^{(i)}}\right)\right. \\ &\quad \left.\left. + 2\Lambda^{(i)}\left(r_i^{1+n_j^{(i)}} - r_{i-1}^{1+n_j^{(i)}}\right)\right)\right], \end{aligned} \tag{32}$$

where

$$\begin{aligned} \Lambda_1^{(i)} &= C_{13}^{(i)}\Lambda^{(i)} + C_{23}^{(i)}\Lambda^{(i)} + C_{33}^{(i)}\varepsilon_0, \\ \Lambda_2^{(i)} &= C_{11}^{(i)}\Lambda^{(i)} + C_{12}^{(i)}\Lambda^{(i)} + C_{13}^{(i)}\varepsilon_0, \end{aligned} \tag{33}$$

and

$$K_j^{(i)} = \begin{cases} \frac{r_i^{1+n_j^{(i)}} - r_{i-1}^{1+n_j^{(i)}}}{1+n_j^{(i)}}, & n_j^{(i)} \neq -1, \\ \ln(r_i) - \ln(r_{i-1}), & n_j^{(i)} = -1. \end{cases} \tag{34}$$

The homogenized cylinder is described by the same equations with the layers 1 and N, with the difference that the (i) must be replaced by eff.

For the effective medium, the boundary conditions for the axial Young's modulus give $D_1^{\text{eff}} = -C_{13}^{\text{eff}}\varepsilon_0 \Big/ \left(C_{11}^{\text{eff}} + C_{12}^{\text{eff}}\right)$ and

$$W^{\text{eff}} = \frac{1}{2}\left\langle \sigma_{rr}^{\text{eff}}\varepsilon_{rr}^{\text{eff}} + \sigma_{\theta\theta}^{\text{eff}}\varepsilon_{\theta\theta}^{\text{eff}} + \sigma_{zz}^{\text{eff}}\varepsilon_{zz}^{\text{eff}}\right\rangle = \frac{1}{2}E_3^{\text{eff}}\varepsilon_0^2. \tag{35}$$

Since $W^{\text{RVE}} = W^{\text{eff}}$, we get

$$\begin{aligned} E_3^{\text{eff}} &= \frac{2}{\varepsilon_0^2 r_N^2}\sum_{i=1}^{N}\left[\left(\Lambda_1^{(i)}\varepsilon_0 + 2\Lambda_2^{(i)}\Lambda^{(i)}\right)\frac{r_i^2 - r_{i-1}^2}{2} + 2\varepsilon_0\sum_{j=1}^{2}D_j^{(i)}\left(C_{23}^{(i)} + n_j^{(i)}C_{13}^{(i)}\right)K_j^{(i)}\right. \\ &\quad \left. + \sum_{j=1}^{2}\left(\frac{C_{22}^{(i)}}{n_j^{(i)}} + C_{12}^{(i)}\right)D_j^{(i)}\left(D_j^{(i)}\left(r_i^{2n_j^{(i)}} - r_{i-1}^{2n_j^{(i)}}\right) + 2\Lambda^{(i)}\left(r_i^{1+n_j^{(i)}} - r_{i-1}^{1+n_j^{(i)}}\right)\right)\right]. \end{aligned} \tag{36}$$

For the effective medium, the boundary conditions for the axial stiffness component give $D_1^{\text{eff}} = 0$ and

$$W^{\text{eff}} = \frac{1}{2}\left\langle \sigma_{rr}^{\text{eff}}\varepsilon_{rr}^{\text{eff}} + \sigma_{\theta\theta}^{\text{eff}}\varepsilon_{\theta\theta}^{\text{eff}} + \sigma_{zz}^{\text{eff}}\varepsilon_{zz}^{\text{eff}}\right\rangle = \frac{1}{2}C_{33}^{\text{eff}}\varepsilon_0^2. \tag{37}$$

Since $W^{\text{RVE}} = W^{\text{eff}}$, we get

$$\begin{aligned} C_{33}^{\text{eff}} &= \frac{2}{\varepsilon_0^2 r_N^2}\sum_{i=1}^{N}\left[\left(\Lambda_1^{(i)}\varepsilon_0 + 2\Lambda_2^{(i)}\Lambda^{(i)}\right)\frac{r_i^2 - r_{i-1}^2}{2} + 2\varepsilon_0\sum_{j=1}^{2}D_j^{(i)}\left(C_{23}^{(i)} + n_{ji}C_{13}^{(i)}\right)K_j^{(i)}\right. \\ &\quad \left. + \sum_{j=1}^{2}\left(\frac{C_{22}^{(i)}}{n_j^{(i)}} + C_{12}^{(i)}\right)D_j^{(i)}\left(D_j^{(i)}\left(r_i^{2n_j^{(i)}} - r_{i-1}^{2n_j^{(i)}}\right) + 2\Lambda^{(i)}\left(r_i^{1+n_j^{(i)}} - r_{i-1}^{1+n_j^{(i)}}\right)\right)\right]. \end{aligned} \tag{38}$$

3.4. In-plane shear modulus

The composite cylinders method proposed by Hashin Rosen [20] can provide only bounds for the in-plane shear modulus μ_{12}^{eff}. For this reason we will use the generalized self consistent composite cylinders method, proposed by Christensen [7]. In this case, an additional layer (layer $N+1$) is added, representing the effective medium with external radius $r_{N+1} \to \infty$. The admissible displacement field for this case is described by the equations

$$u_r^{(i)} = \sum_{j=1}^{4} a_j^{(i)} D_j^{(i)} r^{n_j^{(i)}} \sin(2\theta),$$

$$u_r^{(N+1)} = \varepsilon_0 \frac{r_N}{4\mu_{12}^{\text{eff}}} \left(\frac{2r}{r_N} + D_3^{(N+1)} \frac{r_N^3}{r^3} + 2\left(1 + \frac{\mu_{12}^{\text{eff}}}{K_{12}^{\text{eff}}}\right) D_4^{(N+1)} \frac{r_N}{r} \right) \sin(2\theta),$$

$$u_\theta^{(i)} = \sum_{j=1}^{4} D_j^{(i)} r^{n_j^{(i)}} \cos(2\theta),$$

$$u_\theta^{(N+1)} = \varepsilon_0 \frac{r_N}{4\mu_{12}^{\text{eff}}} \left(\frac{2r}{r_N} - D_3^{(N+1)} \frac{r_N^3}{r^3} + \frac{\mu_{12}^{\text{eff}}}{K_{12}^{\text{eff}}} D_4^{(N+1)} \frac{r_N}{r} \right) \cos(2\theta),$$

$$u_z^{(j)} = 0, \quad \text{for } i = 1, \ldots, N, \; j = 1, \ldots, 4, \tag{39}$$

with

$$\alpha_j^{(i)} = 2 \frac{C_{22}^{(i)} + C_{66}^{(i)} - n_j^{(i)} \left(C_{12}^{(i)} + C_{66}^{(i)} \right)}{C_{22}^{(i)} + 4C_{66}^{(i)} - \left(n_j^{(i)} \right)^2 C_{11}^{(i)}}, \quad \text{for } i = 1, \ldots, N,$$
$$j = 1, \ldots, 4. \tag{40}$$

The exponents $n_j^{(i)}$, $j = 1, \ldots, 4$ are the solutions of the polynomial

$$An^4 - Bn^2 + \Gamma = 0, \tag{41}$$

where

$$A = C_{11}^{(i)} C_{66}^{(i)},$$
$$B = \left(C_{11}^{(i)} + C_{22}^{(i)} - 8C_{12}^{(i)} \right) C_{66}^{(i)} + 4\left(C_{11}^{(i)} C_{22}^{(i)} - \left(C_{12}^{(i)} \right)^2 \right), \tag{42}$$
$$\Gamma = 9C_{22}^{(i)} C_{66}^{(i)}.$$

The $n_1^{(i)}$, $n_2^{(i)}$ are the positive solutions, while the $n_3^{(i)}$, $n_4^{(i)}$ are the negative solutions. If z is the axis of symmetry for the layer (i.e. the axis of the fiber), these equations reduce to the equations given in Seidel and Lagoudas [47], therefore the extra complication is directly attributed to the difference in material symmetry orientation of the interphase layer, which is transversely isotropic with axis of symmetry parallel to the radial direction (i.e. the direction of the microfibers).

The external boundary conditions are already included in the displacement field of the $N+1$ layer. We also need the conditions ensuring boundness at the origin

$$D_3^{(1)} = D_4^{(1)} = 0, \tag{43}$$

and the continuity conditions

$$u_r^{(i)}(r_i) = u_r^{(i+1)}(r_i), \quad u_\theta^{(i)}(r_i) = u_\theta^{(i+1)}(r_i),$$
$$\sigma_{rr}^{(i)}(r_i) = \sigma_{rr}^{(i+1)}(r_i), \quad \sigma_{r\theta}^{(i)}(r_i) = \sigma_{r\theta}^{(i+1)}(r_i), \quad \text{for } i = 1, \ldots, N. \tag{44}$$

Finally, the strain energy equivalency is written

$$\int_0^{2\pi} \left[\sigma_{rr}^{(N+1)} u_r^{\text{eff}} + \sigma_{r\theta}^{(N+1)} u_\theta^{\text{eff}} - \left(\sigma_{rr}^{\text{eff}} u_r^{(N+1)} + \sigma_{r\theta}^{\text{eff}} u_\theta^{(N+1)} \right) \right]_{r=r_N} d\theta = 0. \tag{45}$$

Eq. (45) is the interaction (surface) energy form converted from the volume averaged form. The surface energy form arises from the strain energy equality between the composite and the homogenized medium [7, pp. 55–56] and it provides easier computations than using directly the stored strain energy equivalency.

The displacement field of the effective medium is

$$u_r^{\text{eff}} = \frac{r \sin(2\theta)}{2\mu_{12}^{\text{eff}}}, \quad u_\theta^{\text{eff}} = \frac{r \cos(2\theta)}{2\mu_{12}^{\text{eff}}}, \quad u_z^{\text{eff}} = 0. \tag{46}$$

The strain energy equivalency leads to the final condition that

$$D_4^{(N+1)} = 0, \tag{47}$$

from which we solve for μ_{12}^{eff}.

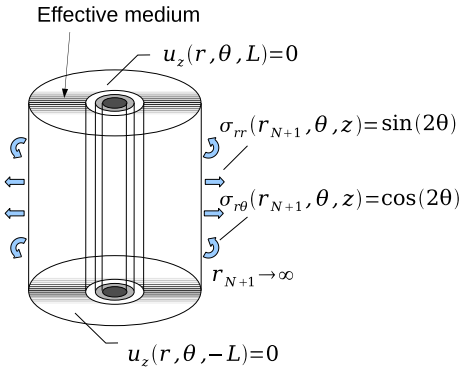

Fig. 7. Generalized self consistent method for in-plane shear modulus.

It needs to be mentioned that, even though displacement fields for similar boundary value problems with the one of Fig. 7 have been introduced in the literature, this is the first time that the in-plane shear modulus is obtained using the displacement field of Eq. (39) and the Christensen's approach.

The generalized self consistent composite cylinders method can also be used to obtain the other effective properties (in plane bulk modulus, axial shear modulus, axial Young's modulus and axial stiffness component). In these cases, iterative schemes need to be employed, since the generalized self consistent composite cylinders method leads to nonlinear equations. The values of these properties, obtained by the later method, are in very good agreement with the values obtained by the composite cylinders method [46], indicating that the luck of use of the effective layer in obtaining these properties is an acceptable simplification.

3.5. Other material properties

The effective axial Poisson's ratio is computed from the relation

$$\nu_{23}^{\text{eff}} = \sqrt{\frac{C_{33}^{\text{eff}} - E_3^{\text{eff}}}{4K_{12}^{\text{eff}}}}. \tag{48}$$

The effective in-plane Poisson's ratio is computed from the relation

$$\nu_{12}^{\text{eff}} = \frac{K_{12}^{\text{eff}} - \mu_{12}^{\text{eff}} - 4\left(\nu_{23}^{\text{eff}}\right)^2 \mu_{12}^{\text{eff}} K_{12}^{\text{eff}} / E_3^{\text{eff}}}{K_{12}^{\text{eff}} + \mu_{12}^{\text{eff}} + 4\left(\nu_{23}^{\text{eff}}\right)^2 \mu_{12}^{\text{eff}} K_{12}^{\text{eff}} / E_3^{\text{eff}}}. \tag{49}$$

The effective in-plane Young's modulus is computed from the relation

$$E_1^{\text{eff}} = \frac{4\mu_{12}^{\text{eff}} K_{12}^{\text{eff}}}{K_{12}^{\text{eff}} + \mu_{12}^{\text{eff}} + 4\left(\nu_{23}^{\text{eff}}\right)^2 \mu_{12}^{\text{eff}} K_{12}^{\text{eff}} / E_3^{\text{eff}}}. \tag{50}$$

The effective properties described in this section are related with unidirectional "fuzzy fiber" composites. One can identify the effective properties of the "fuzzy fiber" alone, using the generalized self consistent composite cylinder method, by considering almost zero matrix layer (layer with $N = 3$). This information is necessary if we need the "fuzzy fiber" properties for use in other methods such as the Mori–Tanaka for addressing composites with multiple inhomogeneity types.

4. Effective properties of composites with multiple types of "fuzzy fibers"

In the previous sections we dealt with unidirectional "fuzzy fiber" composites, when only one type of "fuzzy fiber" is considered. However, in order to consider more complicated structures

(for instance, "fuzzy fibers" with different orientations or different materials for the fibers, "fuzzy fibers" with various CNT concentrations), the knowledge of the effective properties of the "fuzzy fiber" itself must be combined with the knowledge of the strain or stress concentration tensors.

4.1. General relations for composites with multiple "fuzzy fiber" types

In the case of multiple "fuzzy fiber" types, each type defines a different phase in the composite. Assuming $J = 1, 2, \ldots, \mathfrak{D}$ distinct fiber types, with volume fractions c^J and stiffness tensors C^J_{ijkl}, the effective behavior of the final composite is identified by the relation

$$C^{\text{eff}}_{ijkl} = C^m_{ijkl} + \sum_{J=1}^{\mathfrak{D}} c^J \left(C^J_{ijop} - C^m_{ijop} \right) A^J_{opkl}, \tag{51}$$

where A^J_{opkl} is the strain concentration tensor of each phase and the index m denotes the matrix phase. The relation that holds for the volume fractions is

$$c^m + \sum_{J=1}^{\mathfrak{D}} c^J = 1. \tag{52}$$

The composite cylinders method introduced in the previous section allows us to compute the stress concentration tensor of aligned "fuzzy fiber" composites. The components of the stress concentration tensor B^J_{ijkl} connect the volume average of the stress $\sigma^{\text{Total}}_{ij}$ over the three material layers (i.e, the fiber, the reinforced interphase and the matrix) with the volume average of the stress σ^J_{ij} over only the fiber and the reinforced interphase through the relation

$$\left\langle \sigma^J_{ij} \right\rangle = B^J_{ijkl} \langle \sigma^{\text{Total}}_{kl} \rangle. \tag{53}$$

It should be noted that the stress concentration tensor is most conveniently applied in Cartesian coordinates. So the components of stresses in Eq. (53) must be expressed in the Cartesian coordinate system. The analytical forms of the stress concentration expressions (volume averages of σ^J_{ijkl} and $\sigma^{\text{Total}}_{ijkl}$) for all the solved boundary value problems are presented in Appendix C.

Since in four out of five properties we use the composite cylinders method as opposed to the generalized self consistent composite cylinders method, the method we propose is quasi-dilute in that the interactions between the various types or orientations of fibers are not directly accounted for.[1] This can be adjusted for by taking the computed composite cylinders concentration tensor components to be the dilute concentration tensor components (the difference between the quasi-dilute and the dilute is only on the in-plane shear term). The dilute concentration tensor H^J_{ijkl} of a "fuzzy fiber" composite can be identified using the composite cylinders method and considering very large matrix volume fraction (third layer). The obtained tensor relates the stress in the inhomogeneity to the uniform stress in the far field applied traction.

Using five appropriate boundary value problems and geometric symmetry considerations, the components of the dilute stress concentration tensor can be uniquely defined from the proposed composite cylinders method. However, the sets of equations produced by the in-plane bulk modulus test and the axial stiffness component are not linearly independent, and therefore an additional boundary value problem to those described above is needed. This additional problem, the transverse extension test, is presented in Appendix B.

[1] In [46] it was observed that the generalized self consistent composite cylinders and composite cylinders methods yield the same effective properties and concentration tensors for aligned fiber composites. So, for aligned composites, composite cylinders is a very good approximation of the generalized self consistent composite cylinders concentration tensor components.

The dilute strain concentration tensor G^J_{ijkl} is computed from the dilute stress concentration tensor H^J_{ijkl} the "fuzzy fiber" stiffness tensor C^J_{ijkl} and the matrix stiffness tensor M^m_{ijkl} through the relation

$$G^J_{ikjl} = \left(C^J_{ikop} \right)^{-1} H^J_{opqr} C^m_{qrjl}. \tag{54}$$

The properties C^J_{ijkl} of the "fuzzy fiber" are computed from the composite cylinders method, imposing essentially the two phase model of carbon fiber and reinforced interphase to make an effective layer.

The computed dilute strain concentration tensor can be used in a Mori–Tanaka method (in order to allow for interactions) to identify the effective properties of a composite with mixed "fuzzy fiber" types. Especially for composites with "fuzzy fibers" of different orientation, Mori–Tanaka is a very efficient and easily implemented micromechanics method, provided one accounts properly for the interactions of the fibers with different orientation (for further details see [11,46]).

According to the Mori–Tanaka method, the strain concentration tensor A^J_{ijkl} for each phase in aligned fiber composites is computed by the relation [38]

$$A^J_{ijkl} = G^J_{ijmn} \left[c^m I_{mnkl} + \sum_{J=1}^{\mathfrak{D}} c^J G^J_{mnkl} \right]^{-1}. \tag{55}$$

Combining (51) and (55), we obtain the effective stiffness tensor for aligned "fuzzy fiber" composites,

$$C^{\text{eff}}_{ijkl} = C^m_{ijkl} + \sum_{J=1}^{\mathfrak{D}} c^J \left(C^J_{ijop} - C^m_{ijop} \right) G^J_{opmn} \left[c^m I_{mnkl} + \sum_{J=1}^{\mathfrak{D}} c^J G^J_{mnkl} \right]^{-1}. \tag{56}$$

When the "fuzzy fibers" have different orientation, the strain concentration tensor A^J_{ijkl} for each phase is computed by the relation [11,46]

$$A^J_{ijkl} = Q^J_{ia} Q^J_{jb} Q^J_{mc} Q^J_{nd} G^J_{abcd} \left[c^m I_{mnkl} + \sum_{J=1}^{\mathfrak{D}} c^J Q^J_{me} Q^J_{nf} Q^J_{kg} Q^J_{lh} G^J_{efgh} \right]^{-1}, \tag{57}$$

where Q^J_{ij} is the rotation tensor of the fiber. Combining (51) and (57), we obtain the effective stiffness tensor

$$C^{\text{eff}}_{ijkl} = C^m_{ijkl} + \sum_{J=1}^{\mathfrak{D}} c^J \left(C^J_{ijop} - C^m_{ijop} \right) Q^J_{oa} Q^J_{pb} Q^J_{mc} Q^J_{nd} G^J_{abcd} \times \left[c^m I_{mnkl} + \sum_{J=1}^{\mathfrak{D}} c^J Q^J_{me} Q^J_{nf} Q^J_{kg} Q^J_{lh} G^J_{efgh} \right]^{-1}. \tag{58}$$

4.2. Special cases of composites

Based on the relations described in the previous subsection, we can provide expressions of the effective properties for special cases of composites with "fuzzy fibers".

4.2.1. Aligned fiber composites with one "fuzzy fiber" type

In the case of aligned fiber composites with only one type of "fuzzy fibers" the effective behavior is directly computed by the proposed composite cylinders method. Alternatively, using the Mori–Tanaka method, the effective stiffness tensor is identified by the relation

$$C^{\text{eff}}_{ijkl} = C^m_{ijkl} + c \left(C^f_{ijop} - C^m_{ijop} \right) G^f_{opmn} \left[(1 - c^f) I_{mnkl} + c^f G^f_{mnkl} \right]^{-1}, \tag{59}$$

where the indices f and m denote the "fuzzy fiber" and the matrix respectively.

Table 1
Mechanical properties of constituents.

fiber: T650 carbon fiber (2.5 μm radius) [10]	
Axial Young's modulus	241 GPa
Transverse Young's modulus	14.5 GPa
Axial shear modulus	22.8 GPa
Transverse shear modulus	4.8 GPa
Axial Poisson's ratio	0.27
Matrix: EPIKOTE 862 resin	
Young's modulus	3 GPa
Poisson's ratio	0.3
Microfibers: CNTs	
Young's modulus E	1100 GPa
Poisson's ratio	0.14

Table 2
Mechanical properties of reinforced interphase.

Reinforced interphase (2 μm thickness)	
Axial Young's modulus E_{33}	7.01 GPa
Transverse Young's modulus E_{11}	298.64 GPa
Axial Shear modulus μ_{23}	2.52 GPa
Transverse shear modulus μ_{12}	2.81 GPa
Bulk modulus K_{23}	5.76 GPa

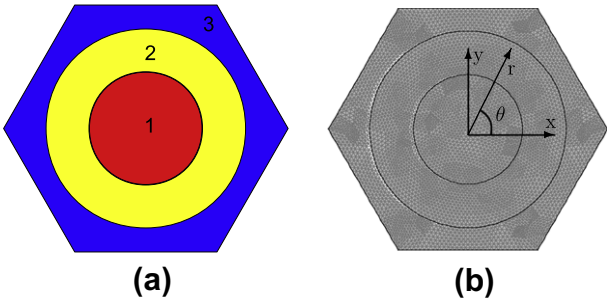

Fig. 8. (a) Unit cell of the "fuzzy fiber": 1 carbon fiber (red), 2 reinforced interphase (yellow) and 3 resin (blue). (b) Finite element mesh of the unit cell.

4.2.2. Composites with randomly oriented "fuzzy fibers"

In the case of composites with random orientation of the fibers, the knowledge of the concentration tensors for composites with aligned fibers is sufficient in order to use the Mori–Tanaka method (details are given in [11,46]. The actual concentration tensor of the phases is provided through a careful averaging of the dilute concentration tensors for aligned fiber composites over all possible orientations. The effective stiffness tensor of a composite with randomly oriented "fuzzy fibers" is given by [11]

$$C_{ijkl}^{\text{eff,ran}} = C_{ijkl}^{m} + \left(C_{ijop}^{f} - C_{ijop}^{m}\right)\left\{\left\{G_{opqr}^{f}\right\}\right\}\left[(1-c^{f})I_{qrkl} + \left\{\left\{G_{qrkl}^{f}\right\}\right\}\right]^{-1}, \tag{60}$$

where $\{\{\phi\}\}$ denotes averaging of function ϕ over all possible orientations and c^f is the fibers volume fraction.

5. Numerical examples

The numerical examples presented in this section are motivated by the experiments presented in [42]. T650 carbon fibers with diameter $D = 5$ μm are coated with radially aligned hollow carbon nanotubes of $d = 2$ μm length (Fig. 1 in [42]). The CNTs have internal radius 0.51 nm and external radius 0.85 nm. The "fuzzy fibers" are embedded in EPIKOTE 862 resin. The reinforced interphase contains CNTs with average volume fraction 42.17%.

For the effective properties of the reinforced interphase, we use the procedure described in Seidel and Lagoudas [47]. The single walled CNTs have the properties of graphite. The reinforced interphase is assumed to behave like a reinforced interphase with aligned CNTs and its effective properties can be obtained using the generalized self consistent composite cylinders method. In this approach we assume that there is perfect bonding between the CNTs and the resin. Esteva Spanos [12] have shown through micromechanics methods that the imperfect bonding affects the composite behavior, especially at high CNT volume fractions. In case that we need to account for the imperfect bonding between the two materials, we have to consider appropriate interfacial conditions, like jump conditions in displacements or tractions.

With regard to the carbon fibers, we consider in this study that they behave as transversely isotropic materials. The mechanical properties of the carbon fibers, the resin and the CNTs are shown in Table 1, while the effective properties of the reinforced interphase are shown in Table 2. In the current modeling we have assumed that the CNTs and the carbon fiber are perfectly bonded. It is known though from several studies that there is usually imperfect bonding between the grown CNTs and the carbon fibers which influences the load transfer between the fibers and the matrix [52,42]. This imperfect bonding has not been quantified, however, and we choose the perfect bonding assumption as an upper bound estimate under the best possible conditions.

In order to check the validity of the proposed method, the results are compared with the effective properties obtained by a numerical method based on the asymptotic expansion homogenization method [45,1,25,8]. The asymptotic expansion homogenization requires a periodic unit cell described in Cartesian coordinate system. The equivalent unit cell for transversely isotropic effective medium is described by a hexagonal structure (Fig. 8a). The program we used for the numerical results is the COMSOL Multiphysics software, using the 2D mesh shown in Fig. 8b. The periodicity in the unit cell is imposed by applying the same displacement field on opposite sides of the hexagon (Fig. 8b). For the purposes of the numerical analysis, we used quadratic Lagrange finite elements. The effective properties of the composite are obtained from the averaged stresses in the unit cell.

In Fig. 9 we show the evolution of the effective properties of the "fuzzy fibers" composite with the increase of the volume fraction of the carbon fibers, maintaining constant reinforced interphase thickness. The large size of the reinforced interphase does not allow the carbon fiber volume fraction to exceed 35%, before reinforced interphases of neighboring carbon fibers come into contact with one another. The maximum carbon fiber volume fraction (close to 25%) presented in Fig. 9 corresponds to 80% volume fraction of "fuzzy fiber" (carbon fiber plus reinforced interphase). As we can observe, the transverse shear modulus and the axial shear modulus are very close for all the volume fractions (despite the fact that this does not hold for the carbon fiber), which is due to the good transverse shear behavior that the intermediate layer has. For high volume fractions, transverse Young's modulus and bulk modulus increase significantly. The results obtained by the numerical method agree very well with the effective properties computed with the proposed composite cylinders method. Small deviations are observed for high volume fractions of carbon fibers. The good agreement between the analytical and the numerical results is consistent with similar observations for carbon nanotube composites [47,19].

The proposed method allows the computation of the strain concentration tensor of a "fuzzy fiber" composite, according to the procedure described in the previous section. Keeping the same dimensions for the carbon fibers and the CNTs and for various volume fractions of the carbon fibers, several terms of the strain concentration tensor are presented in Fig. 10. For comparison reasons,

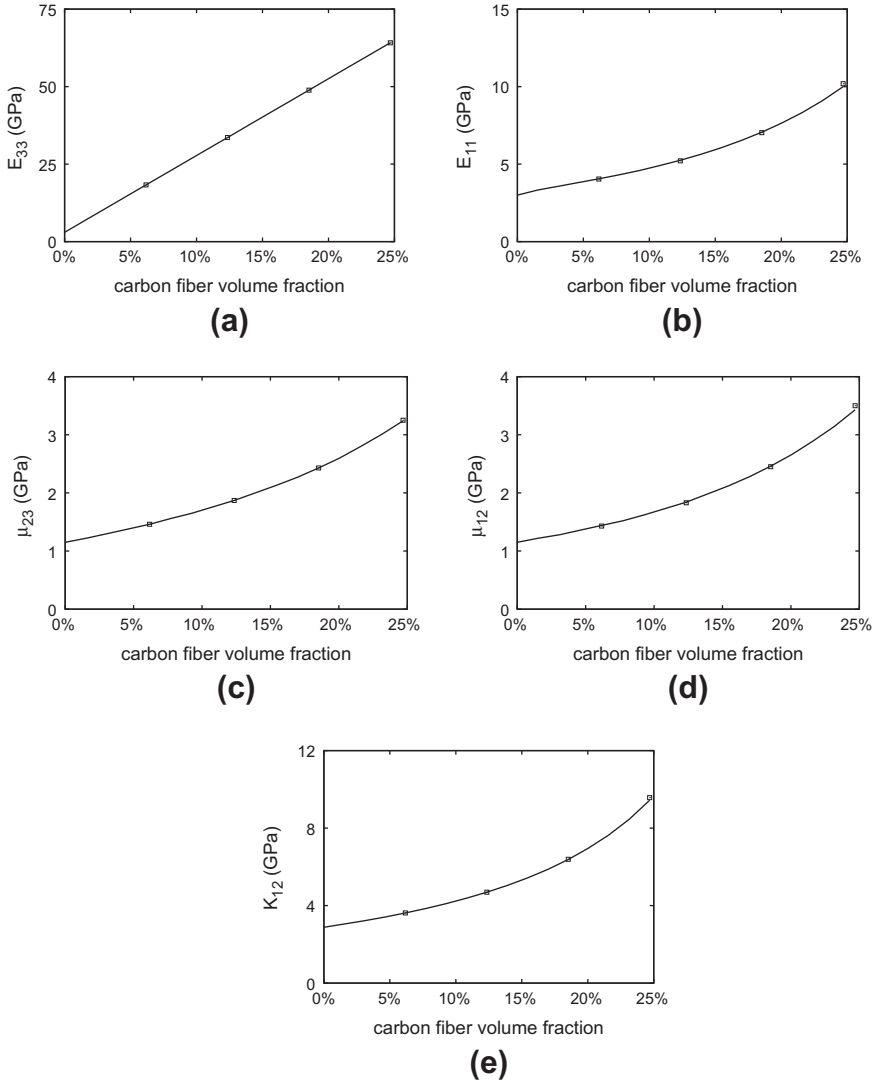

Fig. 9. Mechanical properties of the aligned "fuzzy fiber" composite as a function of the carbon fibers volume fraction. The axial and the transverse properties (solid lines) from the proposed method are compared with FEM results (square points). The thickness of the reinforced interphase is 2 μm.

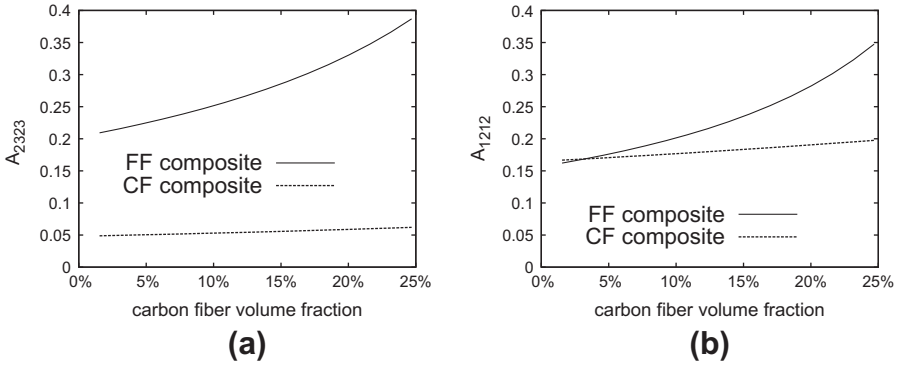

Fig. 10. Strain concentration tensor components for aligned "fuzzy fiber" (FF) composite and carbon fiber (CF) composite.

we also present in the same diagrams the strain concentration tensor components for a carbon fiber composite. The results indicate the significant increase of the shear terms in the strain concentration tensor due to the presence of the reinforced interphase layer. For 60% "fuzzy fiber" volume fraction, the axial shear and the transverse shear terms have an increase of 445% and 41% respectively compared to the case of a carbon fiber composite. We also observe that at very low volume fractions, below 3%, the transverse shear term is slightly lower for the "fuzzy fiber" composite (Fig. 10b). This is perhaps an approximation error due to

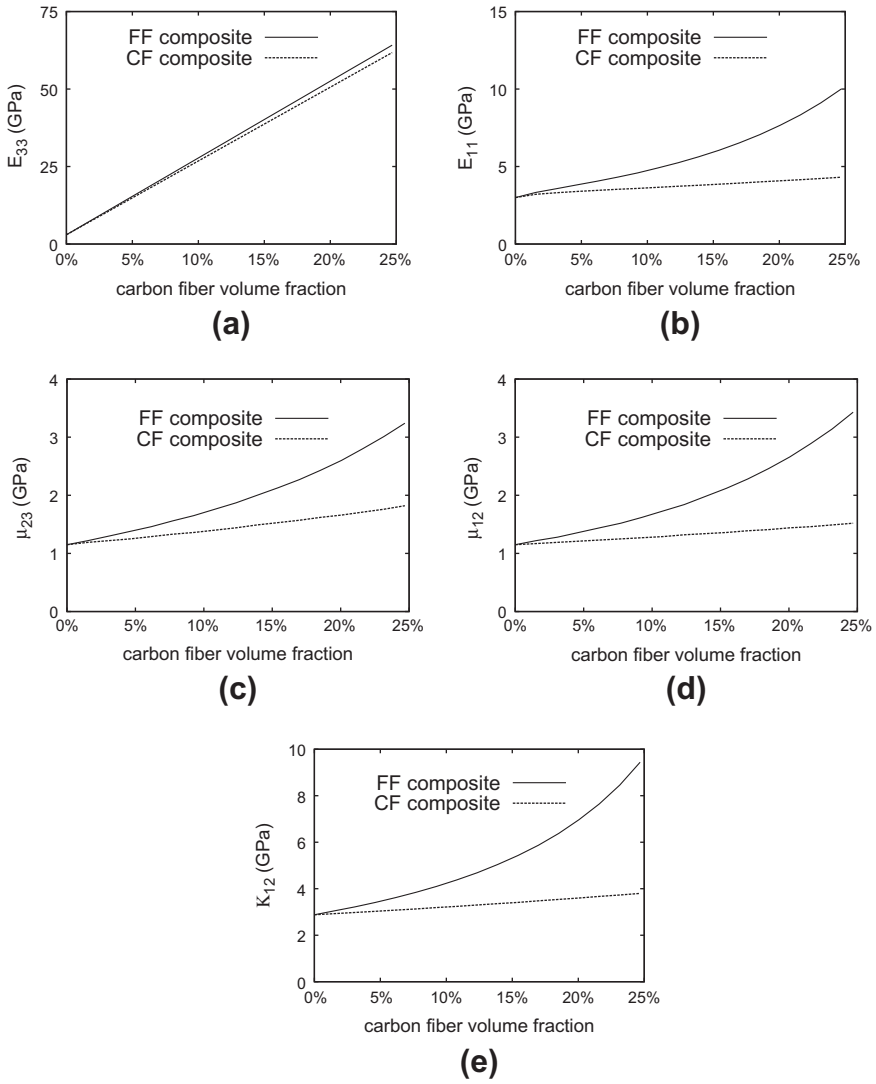

Fig. 11. Comparison between (a) axial Young's modulus, (b) transverse Young's modulus, (c) axial shear modulus, (d) transverse shear modulus and e) transverse bulk modulus of aligned "fuzzy fiber" (FF) composite and carbon fiber (CF) composite. The thickness of the reinforced interphase is 2 μm.

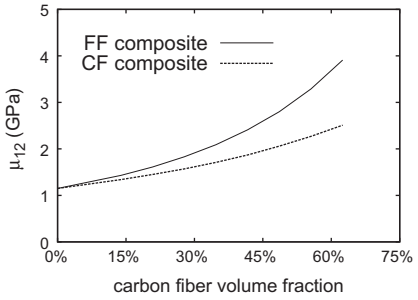

Fig. 12. Comparison between transverse shear modulus of aligned "fuzzy fiber" (FF) composite with small size of reinforced interphase layer (0.5 μm thickness) and carbon fiber (CF) composite.

the use of the quasi-dilute stress concentration tensor, which differs from the dilute stress concentration tensor only on the transverse shear term.

The advantages of the reinforced interphase to the behavior of the composite are represented in Fig. 11. In this Figure we show comparisons of effective properties between "fuzzy fiber" and carbon fiber composites with the same carbon fiber volume fraction. The reinforced interphase does not change the axial properties (Fig. 11a) but enhances significantly the transverse properties. For carbon fiber volume fraction close to 25%, we observe more than 200% increase in transverse Young's modulus and the transverse shear modulus. The enhanced performance of the "fuzzy fiber" composite relative to the carbon fiber is attributed to the high axial stiffness of the CNTs which are oriented in the transverse direction of the "fuzzy fiber" composite. Even in the case that the reinforced interphase is not present and the carbon fiber diameter is extended to provide the same fiber volume fraction with the "fuzzy fiber", the transverse properties remain slightly better for the "fuzzy fiber" composite. For instance, for fiber volume fraction 80%, the effective transverse Young's modulus is 9.58 GPa for the carbon fiber and 10 GPa for the "fuzzy fiber" composite.

Similar results are obtained even if the ratio between carbon fiber diameter to "fuzzy fiber" diameter changes. In Fig. 12 we present the transverse shear modulus of a carbon fiber and a fuzzy fiber composite, when the reinforced interphase layer is small, compared to the carbon fiber (5 μm the diameter of the carbon fiber and 0.5 μm the CNT size). The results (compared to these of Fig. 11d) show similarity, with only a shift in the volume fraction axis. These results clearly show that the ratio between the length of carbon nanotubes and the radius of carbon fiber does not alter the general characteristics in the behavior of the "fuzzy fiber" composite.

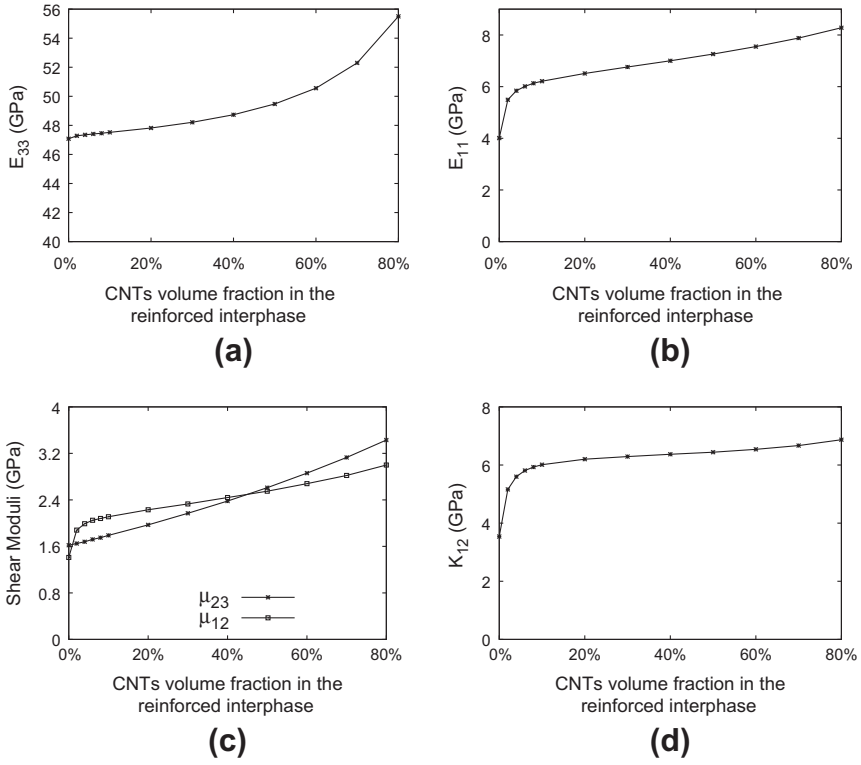

Fig. 13. Effect of CNTs volume fraction in the reinforced interphase on (a) axial Young's modulus, (b) transverse Young's modulus, (c) shear moduli and (d) transverse bulk modulus of aligned "fuzzy fiber" composite. The volume fractions of the carbon fiber and the matrix are 18.5% and 40% respectively. The thickness of the reinforced interphase is 2 μm.

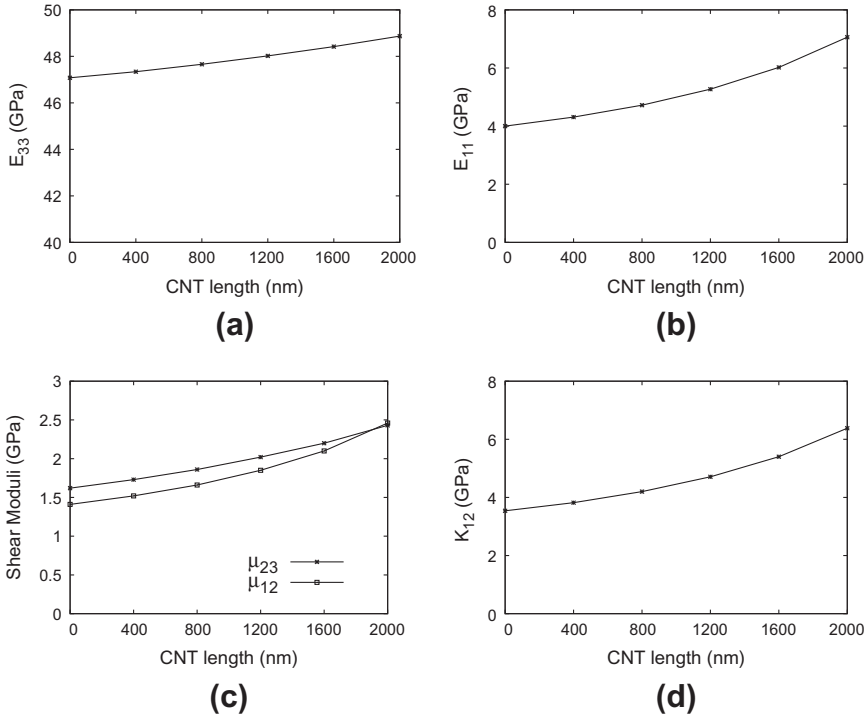

Fig. 14. Effect of CNT length on (a) axial Young's modulus, (b) transverse Young's modulus, (c) shear moduli and (d) transverse bulk modulus of aligned "fuzzy fiber" composite. The carbon fiber volume fraction is 18.5%.

In order to investigate more thoroughly the effect of the reinforced interphase in the mechanical response of the "fuzzy fiber" composite, we perform two cases of parametric analyses.

In the first case we examine the effect of the CNTs volume fraction in the reinforced interphase on the effective behavior of the composite. Keeping the radii of the carbon fiber, the reinforced

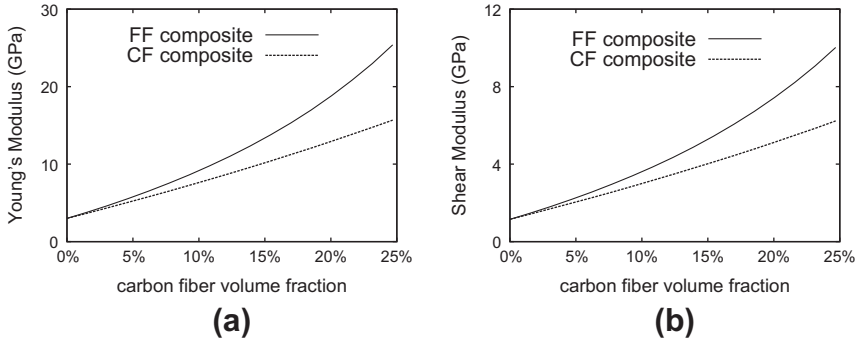

Fig. 15. Comparison of mechanical properties between randomly oriented "fuzzy fiber" (FF) and carbon fiber (CF) composites. The CNTs volume fraction in the reinforced interphase is 42.2%. The thickness of the reinforced interphase in the "fuzzy fiber" is 2 μm.

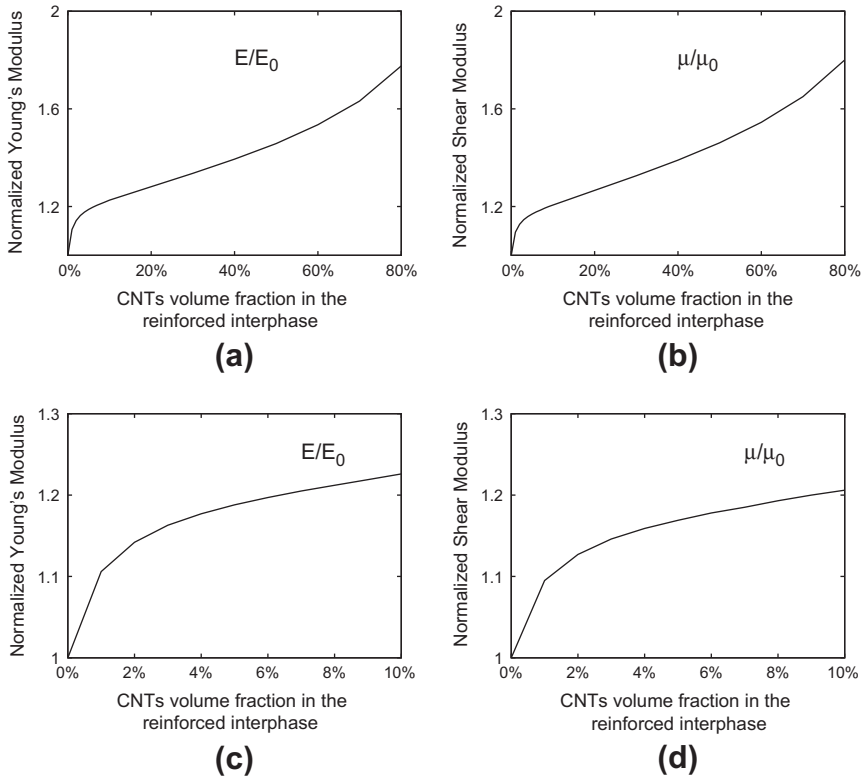

Fig. 16. Effect of CNTs volume fraction in the reinforced interphase on (a) Young's modulus, and (b) shear modulus of randomly oriented "fuzzy fiber" composite. A zoomed area of the same plots at small CNTs volume fractions are presented in (c) and (d) respectively. The index 0 identifies the corresponding mechanical property for carbon fiber composite (without the reinforced interphase layer). The volume fractions of the carbon fiber and the matrix are 18.5% and 40% respectively. The thickness of the reinforced interphase in the "fuzzy fiber" is 2 μm.

interphase and the matrix constant (i.e. holding on composite cylinder scale the volume fractions constant), while varying the local CNT volume fraction within the reinforced interphase, the results are shown in Fig. 13. With regard to the transverse properties, important increase appears only at small CNTs volume fractions. For 10% CNTs volume fraction, the transverse Young's modulus and the transverse shear modulus increase by 55% and 50% respectively compared to no CNTs in the reinforced interphase layer.

In the second case we examine the effect of the length of the CNTs (and eventually the thickness of the reinforced interphase) on the effective behavior of the composite. Keeping the carbon fiber size and the external radius of the matrix constant (i.e. the carbon fiber volume fraction constant), while the reinforced interphase and matrix volume fraction vary, the results are shown in Fig. 14, where we observe that the transverse properties are more affected from the CNT length than the axial properties.

Next, we investigate the effective properties of "fuzzy fiber" composites, where the "fuzzy fibers" have random orientation inside the resin (chopped fibers with high aspect ratio). The obtained effective properties in this case are isotropic, as we should expect, and they are presented in Fig. 15. The presence of the "fuzzy fibers" enhances the properties of the composite, leading to an increase (compared with a randomly oriented carbon fiber composite) of both the Young's modulus and the shear modulus. For 20% carbon fiber volume fraction, the presence of the CNTs in the reinforced interphase provide an increase of 45% in both the effective Young's modulus and the effective shear modulus. The gain however in the

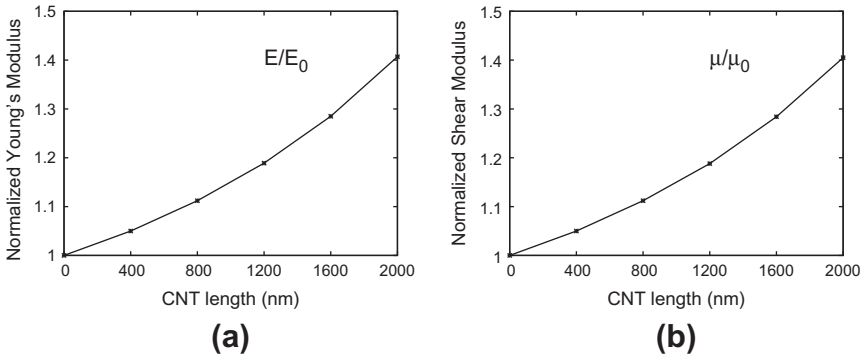

Fig. 17. Effect of CNT length on (a) Young's modulus, and (b) shear modulus of randomly oriented "fuzzy fiber" composite. The index 0 identifies the corresponding mechanical property for carbon fiber composite (without the reinforced interphase layer). The carbon fiber volume fraction is 18.5%.

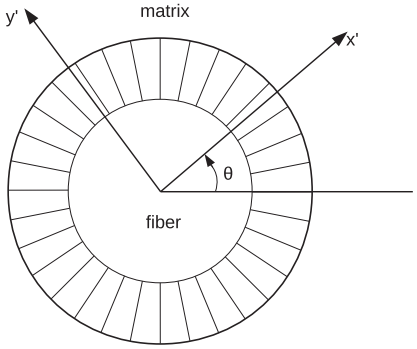

Fig. 18. Orientation indifference of "fuzzy fiber" composite.

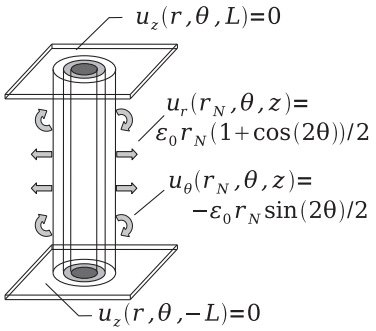

Fig. 19. BVP for transverse extension test.

effective behavior would be significantly greater if the CNTs were randomly oriented and well dispersed in the whole matrix instead of concentrated in a radial orientation in the reinforced interphase. Specifically, the 42.2% volume fraction of CNTs in the reinforced interphase (whose volume fraction in the total composite is 45%), when dispersed in the entire epoxy matrix, corresponds to 23.75% volume fraction of CNTs. By using a combination of the composite cylinders and the Mori–Tanaka methods, as proposed in Seidel and Lagoudas [47], we can obtain the effective behavior (which is isotropic) of the reinforced nanocomposite with CNTs randomly distributed in the matrix. Then, the randomly oriented carbon fibers are embedded in the reinforced with CNTs matrix and the effective properties of the new composite are computed from Eq. (58). For 20% carbon fiber volume fraction, the presence of the CNTs in the entire matrix provide an increase of approximately 125% in both the effective Young's modulus and the effective shear modulus, compared to the randomly oriented fiber composite with CNTs only attached to the carbon fiber. However, this is only a hypothetical case, since it is impossible to fabricate such large well-dispersed volume fractions (viscosity limitations) of CNTs in a polymeric matrix. Moreover, the "fuzzy fiber" material systems are designed to improve the interfacial conditions between carbon fibers and resin and corresponding fracture properties of the composite.

The parametric analysis performed for the aligned fiber composites is now extended to the case of randomly oriented fiber composite.

First, keeping the radii of the carbon fiber, the reinforced interphase and the matrix constant (i.e. holding on composite cylinder scale the volume fractions constant), while varying the local CNT volume fraction within the reinforced interphase, the results are shown in Fig. 16. In this Figure, the Young's and shear moduli are normalized with the corresponding values for a composite with no reinforced interphase layer.

Finally, keeping the carbon fiber size and the external radius of the matrix constant (i.e. the carbon fiber volume fraction constant), while the reinforced interphase and matrix volume fraction vary, the results are shown in Fig. 17. Again, the Young's and shear moduli are normalized with the corresponding values for a composite with no reinforced interphase layer.

In both cases the obtained results present the same pattern with the aligned fiber composite: both the Young and the shear moduli present important increase for small CNTs volume fractions. On the other hand, the increase of the CNT length causes smooth increase in all properties.

6. Conclusions

This paper proposes an extension of the composite cylinders method which allows us to evaluate the effective properties and the concentration tensors of fiber composites, when the fibers are coated with radially aligned nanofibers ("fuzzy fibers"). The in-plane shear modulus is computed using an extension of the Christensen's self consistent composite cylinders method. The developed methodology provides information about the stress and strain concentration tensors, which are essential in sensor applications. Results of the proposed method are compared with numerical methods and showed very good accuracy. In order to assist the design of "fuzzy fiber" composites, the current paper presents extensive parametric studies for composites with aligned and randomly oriented "fuzzy fibers", made of carbon fibers and carbon nanotubes (CNTs), including the effects of CNTs volume fraction and length. The results of the analyses indicate that the coated carbon fibers with CNTs show improved transverse properties compared to uncoated carbon fibers. The CNTs volume fraction, even in small values, has a significant impact on these properties.

Acknowledgements

The authors would like to acknowledge the financial support provided by NSF, Grant No. DMR-0844082 (International Institute for Multifunctional Materials for Energy Conversion – IIMEC Project). The second and third authors would also like to acknowledge the financial support provided by AFOSR through MURI (Synthesis, Characterization and Modeling of Functionally Graded Hybrid Composites for Extreme Environments) Grant FA-9550-09-0686.

Appendix A. Orientation indifference of "fuzzy fiber" composite

In this appendix we compute the mechanical properties of each layer individually at an orthogonal Cartesian coordinate system whose x' axis has an arbitrary angle θ with the horizontal axis (Fig. 18). Since the fiber and the matrix are, at most, transversely isotropic with axis of symmetry parallel to the axis of fiber, their mechanical properties do not depend on the angle θ and they are the same with these presented in Eqs. (1) and (2). The reinforced interphase presents quasi-cylindrically orthotropic behavior, in the sense that it is transversely isotropic with axis of symmetry parallel to the radial direction (Fig. 2). Eq. (3) represents the stiffness tensor of the reinforced interphase in cylindrical coordinates. We can pass from cylindrical to Cartesian coordinate system by proper rotation with respect to the angle θ of Eq. (3). Then we have

$$\begin{pmatrix} \sigma^{int}_{x'x'} \\ \sigma^{int}_{y'y'} \\ \sigma^{int}_{z'z'} \\ \sigma^{int}_{z'y'} \\ \sigma^{int}_{x'z'} \\ \sigma^{int}_{x'y'} \end{pmatrix} = \begin{pmatrix} C'^{int}_{11} & C'^{int}_{12} & C'^{int}_{13} & 0 & 0 & C'^{int}_{16} \\ C'^{int}_{12} & C'^{int}_{22} & C'^{int}_{23} & 0 & 0 & C'^{int}_{26} \\ C'^{int}_{13} & C'^{int}_{23} & C'^{int}_{33} & 0 & 0 & C'^{int}_{36} \\ 0 & 0 & 0 & C'^{int}_{44} & C'^{int}_{45} & 0 \\ 0 & 0 & 0 & C'^{int}_{45} & C'^{int}_{55} & 0 \\ C'^{int}_{16} & C'^{int}_{26} & C'^{int}_{36} & 0 & & C'^{int}_{66} \end{pmatrix} \begin{pmatrix} \varepsilon^{int}_{x'x'} \\ \varepsilon^{int}_{y'y'} \\ \varepsilon^{int}_{z'z'} \\ 2\varepsilon^{int}_{z'y'} \\ 2\varepsilon^{int}_{x'z'} \\ 2\varepsilon^{int}_{x'y'} \end{pmatrix},$$

where

$$C'^{int}_{11} = \frac{C^{int}_{11}x'^4 + 2\left(C^{int}_{12} + 2C^{int}_{66}\right)x'^2y'^2 + C^{int}_{22}y'^4}{\left(x'^2 + y'^2\right)^2},$$

$$C'^{int}_{12} = \frac{C^{int}_{12}(x'^4 + y'^4) + \left(C^{int}_{11} + C^{int}_{22} - 4C^{int}_{66}\right)x'^2y'^2}{\left(x'^2 + y'^2\right)^2},$$

$$C'^{int}_{13} = \frac{C^{int}_{13}x'^2 + C^{int}_{23}y'^2}{x'^2 + y'^2},$$

$$C'^{int}_{16} = \frac{\left(C^{int}_{11} - C^{int}_{12} - 2C^{int}_{66}\right)x'^3y' + \left(C^{int}_{12} - C^{int}_{22} + 2C^{int}_{66}\right)x'y'^3}{\left(x'^2 + y'^2\right)^2},$$

$$C'^{int}_{22} = \frac{C^{int}_{11}y'^4 + 2\left(C^{int}_{12} + 2C^{int}_{66}\right)x'^2y'^2 + C^{int}_{22}x'^4}{\left(x'^2 + y'^2\right)^2},$$

$$C'^{int}_{23} = \frac{C^{int}_{13}y'^2 + C^{int}_{23}x'^2}{x'^2 + y'^2},$$

$$C'^{int}_{26} = \frac{\left(C^{int}_{11} - C^{int}_{12} - 2C^{int}_{66}\right)x'y'^3 + \left(C^{int}_{12} - C^{int}_{22} + 2C^{int}_{66}\right)x'^3y'}{\left(x'^2 + y'^2\right)^2},$$

$$C'^{int}_{33} = C^{int}_{33},$$

$$C'^{int}_{36} = \frac{\left(C^{int}_{13} - C^{int}_{23}\right)x'y'}{x'^2 + y'^2},$$

$$C'^{int}_{44} = \frac{C^{int}_{44}x'^2 + C^{int}_{55}y'^2}{x'^2 + y'^2},$$

$$C'^{int}_{45} = \frac{\left(C^{int}_{55} - C^{int}_{44}\right)x'y'}{x'^2 + y'^2},$$

$$C'^{int}_{55} = \frac{C^{int}_{44}y'^2 + C^{int}_{55}x'^2}{x'^2 + y'^2},$$

$$C'^{int}_{66} = \frac{\left(C^{int}_{11} - 2C^{int}_{12} + C^{int}_{22}\right)x'^2y'^2 + C^{int}_{66}(x'^2 - y'^2)^2}{\left(x'^2 + y'^2\right)^2}.$$

The representation of the stiffness tensor C' takes at any angle θ similar form in Cartesian coordinates. For instance, for every θ, the stiffness tensor at a local position $y' = 0$ (position on the axis x') takes the form

$$\mathbf{C}' = \begin{pmatrix} C^{int}_{11} & C^{int}_{12} & C^{int}_{12} & 0 & 0 & 0 \\ C^{int}_{12} & C^{int}_{22} & C^{int}_{23} & 0 & 0 & 0 \\ C^{int}_{12} & C^{int}_{23} & C^{int}_{22} & 0 & 0 & 0 \\ 0 & 0 & 0 & \frac{C^{int}_{22} - C^{int}_{23}}{2} & 0 & 0 \\ 0 & 0 & 0 & 0 & C^{int}_{66} & 0 \\ 0 & 0 & 0 & 0 & & C^{int}_{66} \end{pmatrix},$$

which does not depend on the angle θ. Due to the circular structure of the reinforced interphase, its average behavior (average stiffness tensor over all angles θ) is transversely isotropic with axis of symmetry parallel to the axis of the fiber (axis z of Fig. 1).

Appendix B. Transverse extension test

In order to compute the necessary fifth set of equations for the dilute stress concentration tensor for an aligned "fuzzy fiber" composite, we need to solve an additional boundary value problem, the transverse extension test. The displacement field for the transverse extension test is a superposition of the displacement fields of a) the in-plane bulk modulus and b) the in-plane shear modulus.

We assume the displacement field

$$\begin{aligned} u^{(i)}_r &= \sum_{j=1}^{4} D^{(i)}_j r^{n^{(i)}_j} \cos(2\theta) + \sum_{j=5}^{6} D^{(i)}_j r^{n^{(i)}_j}, \\ u^{(i)}_\theta &= \sum_{j=1}^{4} a^{(i)}_j D^{(i)}_j r^{n^{(i)}_j} \sin(2\theta), \\ u^{(i)}_z &= 0, \quad \text{for } i = 1, \ldots, N, \end{aligned} \tag{B.1}$$

with

$$\alpha^{(i)}_j = -\frac{1}{2}\frac{C^{(i)}_{22} + 4C^{(i)}_{66} - \left(n^{(i)}_j\right)^2 C^{(i)}_{11}}{C^{(i)}_{22} + C^{(i)}_{66} - n^{(i)}_j\left(C^{(i)}_{12} + C^{(i)}_{66}\right)}, \quad \text{for } i = 1, \ldots, N, \quad j = 1, \ldots, 4, \tag{B.2}$$

and $n^{(i)}_j$, $j = 1, \ldots, 4$, the solutions of the polynomial

$$An^4 - Bn^2 + \Gamma = 0, \tag{B.3}$$

where

$$\begin{aligned} A &= C^{(i)}_{11}C^{(i)}_{66}, \\ B &= \left(C^{(i)}_{11} + C^{(i)}_{22} - 8C^{(i)}_{12}\right)C^{(i)}_{66} + 4\left(C^{(i)}_{11}C^{(i)}_{22} - \left(C^{(i)}_{12}\right)^2\right), \\ \Gamma &= 9C^{(i)}_{22}C^{(i)}_{66}. \end{aligned} \tag{B.4}$$

The $n^{(i)}_1$, $n^{(i)}_2$ are the positive solutions, while the $n^{(i)}_3$, $n^{(i)}_4$ are the negative solutions. Moreover

$$n^{(i)}_5 = -n^{(i)}_6 = \sqrt{C^{(i)}_{22}/C^{(i)}_{11}}. \tag{B.5}$$

The boundary conditions of the problem are shown in Fig. 19 (see also [47]). We also need the conditions ensuring bounding at the origin

$$D_3^{(1)} = D_4^{(1)} = D_6^{(1)} = 0, \tag{B.6}$$

and the continuity conditions

$$\begin{aligned} &u_r^{(i)}(r_i) = u_r^{(i+1)}(r_i), \quad u_\theta^{(i)}(r_i) = u_\theta^{(i+1)}(r_i), \\ &\sigma_{rr}^{(i)}(r_i) = \sigma_{rr}^{(i+1)}(r_i), \quad \sigma_{r\theta}^{(i)}(r_i) = \sigma_{r\theta}^{(i+1)}(r_i), \quad \text{for } i = 1,\dots,N. \end{aligned} \tag{B.7}$$

From the solution of this boundary value problem we can obtain the volume averages of the stresses $\sigma_{ij}^{\text{Total}}$ and σ_{ij}^{J}, whose formulas are given in Appendix C.

Appendix C. Volume averages of stress components

In this appendix we present the volume averages of stress components that we need in order to compute the stress concentration tensors. In every subsection we present the nonzero strains and stresses in the cylindrical coordinate system. The relation between the stresses in Cartesian (x,y,z) and cylindrical (r,θ,z) coordinate systems are given by the relations

$$\begin{aligned} \sigma_1 &= \sigma_{xx} = \sigma_{rr}\cos^2\theta + \sigma_{\theta\theta}\sin^2\theta - 2\sigma_{r\theta}\sin\theta\cos\theta, \\ \sigma_2 &= \sigma_{yy} = \sigma_{rr}\sin^2\theta + \sigma_{\theta\theta}\cos^2\theta + 2\sigma_{r\theta}\sin\theta\cos\theta, \\ \sigma_3 &= \sigma_{zz}, \\ \sigma_4 &= \sigma_{yz} = \sigma_{rz}\sin\theta + \sigma_{\theta z}\cos\theta, \\ \sigma_5 &= \sigma_{xz} = \sigma_{rz}\cos\theta - \sigma_{\theta z}\sin\theta, \\ \sigma_6 &= \sigma_{xy} = (\sigma_{rr} - \sigma_{\theta\theta})\sin\theta\cos\theta + \sigma_{r\theta}(\cos^2\theta - \sin^2\theta). \end{aligned}$$

In order to compute the average values, the stresses in the Cartesian coordinate system should be expressed with respect to r,θ,z. The volume averaged stresses of the entire RVE, $\langle\sigma_K^{\text{Total}}\rangle$, and of the "fuzzy fiber", $\langle\sigma_K^J\rangle$, are given by

$$\begin{aligned} \langle\sigma_K^{\text{Total}}\rangle &= \frac{1}{2\pi L r_N}\sum_{i=1}^{N}\int_{-L}^{L}\int_0^{2\pi}\int_{r_{i-1}}^{r_1}\sigma_K r\,dr\,d\theta\,dz, \\ \langle\sigma_K^J\rangle &= \frac{1}{2\pi L r_{N-1}}\sum_{i=1}^{N-1}\int_{-L}^{L}\int_0^{2\pi}\int_{r_{i-1}}^{r_1}\sigma_K r\,dr\,d\theta\,dz. \end{aligned}$$

We introduce for all the following cases the notation:

$$K_j^{(i)} = \begin{cases} \dfrac{r_i^{1+n_j^{(i)}} - r_{i-1}^{1+n_j^{(i)}}}{1+n_j^{(i)}}, & n_j^{(i)} \neq -1, \\ \ln(r_i) - \ln(r_{i-1}), & n_j^{(i)} = -1. \end{cases}$$

$$\Psi_j^{(i)} = 2n_j^{(i)}C_{13}^{(i)} + 2C_{23}^{(i)},$$

$$\Omega_j^{(i)} = n_j^{(i)}\left(C_{11}^{(i)} + C_{12}^{(i)}\right) + C_{12}^{(i)} + C_{22}^{(i)}.$$

C.1. In-plane bulk modulus

Nonzero strain and stress components

$$\epsilon_{rr}^{(i)} = \sum_{j=1}^{2} n_j^{(i)} D_j^{(i)} r^{n_j^{(i)}-1}, \quad \epsilon_{\theta\theta}^{(i)} = \sum_{j=1}^{2} D_j^{(i)} r^{n_j^{(i)}-1},$$

$$\sigma_{rr}^{(i)} = \sum_{j=1}^{2} D_j^{(i)}\left(n_j^{(i)}C_{11}^{(i)} + C_{12}^{(i)}\right) r^{n_j^{(i)}-1},$$

$$\sigma_{\theta\theta}^{(i)} = \sum_{j=1}^{2} D_j^{(i)}\left(n_j^{(i)}C_{12}^{(i)} + C_{22}^{(i)}\right) r^{n_j^{(i)}-1},$$

$$\sigma_{zz}^{(i)} = \sum_{j=1}^{2} D_j^{(i)}\left(n_j^{(i)}C_{13}^{(i)} + C_{23}^{(i)}\right) r^{n_j^{(i)}-1},$$

where $n_j^{(i)}$ is given by Eq. (11).

Average stresses (refer to Cartesian system)

$$\langle\sigma_1^{\text{Total}}\rangle = \langle\sigma_2^{\text{Total}}\rangle = \frac{1}{r_N^2}\sum_{i=1}^{N}\sum_{j=1}^{2} D_j^{(i)}\Omega_j^{(i)}K_j^{(i)},$$

$$\left\langle\sigma_1^J\right\rangle = \left\langle\sigma_2^J\right\rangle = \frac{1}{r_{N-1}^2}\sum_{i=1}^{N-1}\sum_{j=1}^{2} D_j^{(i)}\Omega_j^{(i)}K_j^{(i)},$$

$$\langle\sigma_3^{\text{Total}}\rangle = \frac{1}{r_N^2}\sum_{i=1}^{N}\sum_{j=1}^{2} D_j^{(i)}\Psi_j^{(i)}K_j^{(i)}, \quad \left\langle\sigma_3^J\right\rangle = \frac{1}{r_{N-1}^2}\sum_{i=1}^{N-1}\sum_{j=1}^{2} D_j^{(i)}\Psi_j^{(i)}K_j^{(i)}.$$

C.2. Axial shear modulus

Nonzero strain and stress components

$$2\epsilon_{\theta z}^{(i)} = -\sum_{j=1}^{2} D_j^{(i)} r^{n_j^{(i)}-1}\sin\theta, \quad 2\epsilon_{rz}^{(i)} = \sum_{j=1}^{2} D_j^{(i)} n_j^{(i)} r^{n_j^{(i)}-1}\cos\theta,$$

$$\sigma_{\theta z}^{(i)} = -\sum_{j=1}^{2} D_j^{(i)} C_{44}^{(i)} r^{n_j^{(i)}-1}\sin\theta, \quad \sigma_{rz}^{(i)} = \sum_{j=1}^{2} D_j^{(i)} n_j^{(i)} C_{55}^{(i)} r^{n_j^{(i)}-1}\cos\theta.$$

where $n_j^{(i)}$ is given by Eq. (19).

Average stresses (refer to Cartesian system)

$$\langle\sigma_5^{\text{Total}}\rangle = \frac{1}{r_N^2}\sum_{i=1}^{N}\sum_{j=1}^{2} D_j^{(i)}\Xi_j^{(i)}K_j^{(i)}, \quad \left\langle\sigma_5^J\right\rangle = \frac{1}{r_{N-1}^2}\sum_{i=1}^{N-1}\sum_{j=1}^{2} D_j^{(i)}\Xi_j^{(i)}K_j^{(i)},$$

where

$$\Xi_j^{(i)} = n_j^{(i)}C_{55}^{(i)} + C_{44}^{(i)}.$$

C.3. Axial Young's modulus and axial stiffness component

Nonzero strain and stress components

$$\epsilon_{rr}^{(i)} = \Lambda^{(i)} + \sum_{j=1}^{2} D_j^{(i)} n_j^{(i)} r^{n_j^{(i)}-1}, \quad \epsilon_{\theta\theta}^{(i)} = \Lambda^{(i)} + \sum_{j=1}^{2} D_j^{(i)} r^{n_j^{(i)}-1}, \quad \epsilon_{zz}^{(i)} = \varepsilon_0,$$

$$\sigma_{rr}^{(i)} = \Lambda_2^{(i)} + \sum_{j=1}^{2} D_j^{(i)}\left(n_j^{(i)}C_{11}^{(i)} + C_{12}^{(i)}\right) r^{n_j^{(i)}-1},$$

$$\sigma_{\theta\theta}^{(i)} = \Lambda^{(i)}C_{12}^{(i)} + \Lambda^{(i)}C_{22}^{(i)} + \varepsilon_0 C_{23}^{(i)} + \sum_{j=1}^{2} D_j^{(i)}\left(n_j^{(i)}C_{12}^{(i)} + C_{22}^{(i)}\right) r^{n_j^{(i)}-1}, \quad \text{or}$$

$$\sigma_{\theta\theta}^{(i)} = \Lambda_2^{(i)} + \sum_{j=1}^{2} D_j^{(i)}\left(n_j^{(i)}C_{12}^{(i)} + C_{22}^{(i)}\right) r^{n_j^{(i)}-1},$$

$$\sigma_{zz}^{(i)} = \Lambda_1^{(i)} + \sum_{j=1}^{2} D_j^{(i)}\left(n_j^{(i)}C_{13}^{(i)} + C_{23}^{(i)}\right) r^{n_j^{(i)}-1}.$$

where $\Lambda^{(i)}$, $n_j^{(i)}$, $\Lambda_1^{(i)}$ and $\Lambda_2^{(i)}$ are given by Eqs. (26), (27) and (33).

Average stresses (refer to Cartesian system)

$$\langle\sigma_1^{\text{Total}}\rangle = \frac{1}{r_N^2}\sum_{i=1}^{N}\left[\Lambda_2^{(i)}\left(r_i^2 - r_{i-1}^2\right) + \sum_{j=1}^{2} D_j^{(i)}\Omega_j^{(i)}K_j^{(i)}\right],$$

$$\left\langle\sigma_1^J\right\rangle = \frac{1}{r_{N-1}^2}\sum_{i=1}^{N-1}\left[\Lambda_2^{(i)}\left(r_i^2 - r_{i-1}^2\right) + \sum_{j=1}^{2} D_j^{(i)}\Omega_j^{(i)}K_j^{(i)}\right],$$

$$\langle\sigma_2^{\text{Total}}\rangle = \langle\sigma_1^{\text{Total}}\rangle, \left\langle\sigma_2^J\right\rangle = \left\langle\sigma_1^J\right\rangle,$$

$$\langle\sigma_3^{\text{Total}}\rangle = \frac{1}{r_N^2}\sum_{i=1}^{N}\left[\Lambda_1^{(i)}\left(r_i^2 - r_{i-1}^2\right) + \sum_{j=1}^{2} D_j^{(i)}\Psi_j^{(i)}K_j^{(i)}\right],$$

$$\left\langle\sigma_3^J\right\rangle = \frac{1}{r_{N-1}^2}\sum_{i=1}^{N-1}\left[\Lambda_1^{(i)}\left(r_i^2 - r_{i-1}^2\right) + \sum_{j=1}^{2} D_j^{(i)}\Psi_j^{(i)}K_j^{(i)}\right].$$

C.4. In-plane shear modulus

Nonzero strain and stress components (we refer only to the real layers, not the effective)

$$\epsilon_{rr}^{(i)} = \sum_{j=1}^{4} D_j^{(i)} n_j^{(i)} a_j^{(i)} r^{n_j^{(i)}-1}\sin(2\theta), \epsilon_{\theta\theta}^{(i)} = \sum_{j=1}^{4} D_j^{(i)}\left(a_j^{(i)} - 2\right) r^{n_j^{(i)}-1}\sin(2\theta),$$

$$2\epsilon_{r\theta}^{(i)} = \sum_{j=1}^{4} D_j^{(i)}\left(2a_j^{(i)} + n_j^{(i)} - 1\right) r^{n_j^{(i)}-1}\cos(2\theta),$$

$$\sigma_{rr}^{(i)} = \sum_{j=1}^{4} D_j^{(i)}\left(C_{11}^{(i)} n_j^{(i)} a_j^{(i)} + C_{12}^{(i)} a_j^{(i)} - 2C_{12}^{(i)}\right) r^{n_j^{(i)}-1}\sin(2\theta),$$

$$\sigma_{\theta\theta}^{(i)} = \sum_{j=1}^{4} D_j^{(i)}\left(C_{12}^{(i)} n_j^{(i)} a_j^{(i)} + C_{22}^{(i)} a_j^{(i)} - 2C_{22}^{(i)}\right) r^{n_j^{(i)}-1}\sin(2\theta),$$

$$\sigma_{zz}^{(i)} = \sum_{j=1}^{4} D_j^{(i)}\left(C_{13}^{(i)} n_j^{(i)} a_j^{(i)} + C_{23}^{(i)} a_j^{(i)} - 2C_{23}^{(i)}\right) r^{n_j^{(i)}-1}\sin(2\theta),$$

$$\sigma_{r\theta}^{(i)} = \sum_{j=1}^{4} D_j^{(i)}\left(2a_j^{(i)} + n_j^{(i)} - 1\right) C_{66}^{(i)} r^{n_j^{(i)}-1}\cos(2\theta),$$

where $a_j^{(i)}$ and $n_j^{(i)}$ are defined from Eqs. (40) and (41).

Average stresses (refer to Cartesian system)

$$\langle\sigma_6^{\text{Total}}\rangle = \frac{1}{2r_N^2}\sum_{i=1}^{N}\sum_{j=1}^{4} D_j^{(i)}\Phi_j^{(i)}K_j^{(i)}, \quad \left\langle\sigma_6^J\right\rangle = \frac{1}{2r_{N-1}^2}\sum_{i=1}^{N-1}\sum_{j=1}^{4} D_j^{(i)}\Phi_j^{(i)}K_j^{(i)},$$

where

$$\Phi_j^{(i)} = C_{11}^{(i)} n_j^{(i)} a_j^{(i)} + C_{12}^{(i)}\left(a_j^{(i)} - n_j^{(i)} a_j^{(i)} - 2\right) + C_{22}^{(i)}\left(2 - a_j^{(i)}\right) + 2C_{66}^{(i)}\left(2a_j^{(i)} + n_j^{(i)} - 1\right).$$

C.5. Transverse extension test

Nonzero strain and stress components

$$\epsilon_{rr}^{(i)} = \sum_{j=1}^{4} D_j^{(i)} n_j^{(i)} r^{n_j^{(i)}-1}\cos(2\theta) + \sum_{j=5}^{6} D_j^{(i)} n_j^{(i)} r^{n_j^{(i)}-1},$$

$$\epsilon_{\theta\theta}^{(i)} = \sum_{j=1}^{4} D_j^{(i)}\left(1 + 2a_j^{(i)}\right) r^{n_j^{(i)}-1}\cos(2\theta) + \sum_{j=5}^{6} D_j^{(i)} r^{n_j^{(i)}-1},$$

$$2\epsilon_{r\theta}^{(i)} = \sum_{j=1}^{4} D_j^{(i)}\left(-2 + n_j^{(i)} a_j^{(i)} - a_j^{(i)}\right) r^{n_j^{(i)}-1}\sin(2\theta),$$

$$\sigma_{rr}^{(i)} = \sum_{j=1}^{4} D_j^{(i)}\left(C_{11}^{(i)} n_j^{(i)} + C_{12}^{(i)} + 2C_{12}^{(i)} a_j^{(i)}\right) r^{n_j^{(i)}-1}\cos(2\theta) + \sum_{j=5}^{6} D_j^{(i)}\left(C_{11}^{(i)} n_j^{(i)} + C_{12}^{(i)}\right) r^{n_j^{(i)}-1},$$

$$\sigma_{\theta\theta}^{(i)} = \sum_{j=1}^{4} D_j^{(i)}\left(C_{12}^{(i)} n_j^{(i)} + C_{22}^{(i)} + 2C_{22}^{(i)} a_j^{(i)}\right) r^{n_j^{(i)}-1}\cos(2\theta) + \sum_{j=5}^{6} D_j^{(i)}\left(C_{12}^{(i)} n_j^{(i)} + C_{22}^{(i)}\right) r^{n_j^{(i)}-1},$$

$$\sigma_{zz}^{(i)} = \sum_{j=1}^{4} D_j^{(i)}\left(C_{13}^{(i)} n_j^{(i)} + C_{23}^{(i)} + 2C_{23}^{(i)} a_j^{(i)}\right) r^{n_j^{(i)}-1}\cos(2\theta) + \sum_{j=5}^{6} D_j^{(i)}\left(C_{13}^{(i)} n_j^{(i)} + C_{23}^{(i)}\right) r^{n_j^{(i)}-1},$$

$$\sigma_{r\theta}^{(i)} = \sum_{j=1}^{4} D_j^{(i)}\left(-2 + n_j^{(i)} a_j^{(i)} - a_j^{(i)}\right) C_{66}^{(i)} r^{n_j^{(i)}-1}\sin(2\theta),$$

where $a_j^{(i)}$ and $n_j^{(i)}$ are defined from equations (B.2), (B.3) and (B.5).

Average stresses (refer to Cartesian system)

$$\langle\sigma_1^{\text{Total}}\rangle = \frac{1}{r_N^2}\sum_{i=1}^{N}\left(\frac{1}{2}\sum_{j=1}^{4} D_j^{(i)} M_j^{(i)} K_j^{(i)} + \sum_{j=5}^{6} D_j^{(i)}\Omega_j^{(i)} K_j^{(i)}\right),$$

$$\left\langle\sigma_1^J\right\rangle = \frac{1}{r_{N-1}^2}\sum_{i=1}^{N-1}\left(\frac{1}{2}\sum_{j=1}^{4} D_j^{(i)} M_j^{(i)} K_j^{(i)} + \sum_{j=5}^{6} D_j^{(i)}\Omega_j^{(i)} K_j^{(i)}\right),$$

$$\langle\sigma_2^{\text{Total}}\rangle = \frac{1}{r_N^2}\sum_{i=1}^{N}\left(-\frac{1}{2}\sum_{j=1}^{4} D_j^{(i)} M_j^{(i)} K_j^{(i)} + \sum_{j=5}^{6} D_j^{(i)}\Omega_j^{(i)} K_j^{(i)}\right),$$

$$\left\langle\sigma_2^J\right\rangle = \frac{1}{r_{N-1}^2}\sum_{i=1}^{N-1}\left(-\frac{1}{2}\sum_{j=1}^{4} D_j^{(i)} M_j^{(i)} K_j^{(i)} + \sum_{j=5}^{6} D_j^{(i)}\Omega_j^{(i)} K_j^{(i)}\right),$$

$$\langle\sigma_3^{\text{Total}}\rangle = \frac{1}{r_N^2}\sum_{i=1}^{N}\sum_{j=5}^{6} D_j^{(i)}\Psi_j^{(i)}K_j^{(i)}, \quad \left\langle\sigma_3^J\right\rangle = \frac{1}{r_{N-1}^2}\sum_{i=1}^{N-1}\sum_{j=5}^{6} D_j^{(i)}\Psi_j^{(i)}K_j^{(i)},$$

where

$$M_j^{(i)} = C_{11}^{(i)} n_j^{(i)} + C_{12}^{(i)}\left(1 + 2a_j^{(i)} - n_j^{(i)}\right) - C_{22}^{(i)}\left(1 + 2a_j^{(i)}\right) - 2C_{66}^{(i)}\left(n_j^{(i)} a_j^{(i)} - a_j^{(i)} - 2\right).$$

References

[1] Bensoussan A, Lions J, Papanicolaou G. Asymptotic methods for periodic structures. North Holland; 1978.

[2] Bower C, Zhu W, Jin S, Zhou O. Plasma-induced alignment of carbon nanotubes. Appl Phys Lett 2000;77(6–7):830–2.

[3] Chatterjee D. Some problems of plane strain in a non-homogeneous isotropic cylinder. Pure Appl Geophys 1970;82(1):34–40.

[4] Chatzigeorgiou G, Charalambakis N, Murat F. Homogenization problems of a hollow cylinder made of elastic materials with discontinuous properties. Int J Solids Struct 2008;45:5165–80.

[5] Chatzigeorgiou G, Efendiev Y, Lagoudas DC. Homogenization of aligned fuzzy fiber composites. Int J Solids Struct 2011;48(19):2668–80.

[6] Chen T, Chung C-T, Lin W-L. A revisit of a cylindrically anisotropic tube subjected to pressuring, shearing, torsion, extension and a uniform temperature change. Int J Solids Struct 2000;37:5143–59.

[7] Christensen RM. Mechanics of composite materials. Dover; 1979.

[8] Chung PW, Tamma KK, Namburu RR. Asymptotic expansion homogenization for heterogeneous media: computational issues and applications. Composites: Part A 2001;32:1291–301.

[9] Ci L, Zhao Z, Bai J. Direct growth of carbon nanotubes on the surface of ceramic fibers. Carbon 2005;43(4):883–6.

[10] CYTEC. Typical properties for thornel carbon fibers – standard products. BP Amoco Chemicals, 2011. <cytec.com/engineered-materials/downloads/ThornelTP.pdf>.

[11] Entchev P, Lagoudas D. Modeling porous shape memory alloys using micromechanical averaging techniques. Mech Mater 2002;34:1–24.

[12] Esteva M, Spanos PD. Effective elastic properties of nanotube reinforced composites with slightly weakened interfaces. J Mech Mater Struct 2009;4(5):887–900.

[13] Fisher FT, Bradshaw RD, Brinson LC. Effects of nanotube waviness on the modulus of nanotube-reinforced polymers. Appl Phys Lett 2002;80(24):4647–9.
[14] Fisher FT, Bradshaw RD, Brinson LC. Fiber waviness in nanotube-reinforced polymer composites – I: Modulus predictions using effective nanotube properties. Compos Sci Technol 2003;63(11):1689–703.
[15] Frankland S, Harik V, Odegard G, Brenner D, Gates T. The stress–strain behavior of polymer–nanotube composites from molecular dynamics simulation. Compos Sci Technol 2003;63:1655–61.
[16] Frankland S, Harik V, Odegard G, Brenner O, Gates T. 2002. The stress–strain behavior of polymer–nanotube composites from molecular dynamics simulations. Tech. rep., NASA ICASE.
[17] Griebel M, Hamaekers J. Molecular dynamics simulations of the elastic moduli of polymer–carbon nanotube composites. Comput Meth Appl Mech Eng 2004;193:1773–88.
[18] Hadjiev VG, Lagoudas DC, Oh E-S, Thakre P, Davis D, Files BS, et al. Buckling instabilities of octadecylamine functionalized carbon nanotubes embedded in epoxy. Compos Sci Technol 2006;66:128–36.
[19] Hammerand DC, Seidel GD, Lagoudas DC. Computational micromechanics of clustering and interphase effects in carbon nanotube composites. Mech Adv Mater Struct 2007;14(4):277–94.
[20] Hashin Z, Rosen BW. The elastic moduli of fiber-reinforced materials. J Appl Mech 1964;31:223–32.
[21] Horgan C, Chan A. The pressurized hollow cylinder or disk problem for functionally graded isotropic linearly elastic materials. J Elast 1999;55(1):43–59.
[22] Horgan C, Chan A. The stress response of functionally graded isotropic linearly elastic rotating disks. J Elast 1999;55(1):219–30.
[23] Hosseini Kordkheili S, Naghdabadi R. Thermoelastic analysis of a functionally graded rotating disk. Compos Struct 2007;79:508–16.
[24] Iijima S. Helical microtubules of graphitic carbon. Nature 1991;354:56–8.
[25] Kalamkarov AL, Kolpakov AG. Analysis, design and optimization of composite structures. Wiley; 1997.
[26] Kundalwal SI, Ray MC. Micromechanical analysis of fuzzy fiber reinforced composites. Int J Mech Mater Des 2011;7:149–66.
[27] Liu Y, Chen X. Evaluations of the effective material properties of carbon nanotube-based composites using nanoscale representative volume element. Mech Mater 2003;35:69–81.
[28] Lourie O, Wagner H. Transmission electron microscopy observations of fracture of single-wall carbon nanotubes under axial tension. Appl Phys Lett 1998;73(24):3527–9.
[29] Mathur RB, Chatterjee S, Singh BP. Growth of carbon nanotubes on carbon fibre substrates to produce hybrid/phenolic composites with improved mechanical properties. Compos Sci Technol 2008;68:1608–15.
[30] McCarthy B, Coleman J, Czerw R, Dalton A, in het Panhuis M, Maiti A, et al. A microscopic and spectroscopic study of interactions between carbon nanotubes and a conjugated polymer. J Phys Chem B 2002;106:2210–6.
[31] Milo S, Shaffer P, Windle AH. Fabrication and characterization of carbon nanotube/poly(vinyl alcohol) composites. Adv Mater 1999;11(11):937–41.
[32] Nie G, Batra R. Exact solutions and material tailoring for functionally graded hollow circular cylinders. J Elast 2010;99(2):179–201.
[33] Nie G, Batra R. Material tailoring and analysis of functionally graded isotropic and incompressible linear elastic hollow cylinders. Compos Struct 2010;92(2):265–74.
[34] Odegard G, Gates T, Wise K, Park C, Siochi E. Constitutive modeling of nanotube-reinforced polymer composites. Compos Sci Technol 2003;63(11):1671–87.
[35] Peigney A, Laurent C, Flahaut E, Rousset A. Carbon nanotubes in novel ceramic matrix nanocomposites. Ceram Int 2000;26:677–83.
[36] Popov V. Carbon nanotubes: properties and applications. Mater Sci Eng R 2004;43:61–102.
[37] Potschke P, Bhattacharyya AR, Janke A. Carbon nanotube-filled polycarbonate composites produced by melt mixing and their use in blends with polyethylene. Carbon 2004;42:965–9.
[38] Qu J, Cherkaoui M. Fundamentals of micromechanics of solids. Wiley; 2006.
[39] Ray MC. A shear lag model of piezoelectric composite reinforced with carbon nanotubes-coated piezoelectric fibers. Int J Mech Mater Des 2010;6:147–55.
[40] Roche S. Carbon nanotubes: exceptional mechanical and electronic properties. Ann Chem Sci Mater 2000;25:529–32.
[41] Ruhi M, Angoshtari A, Naghdabadi R. Thermoelastic analysis of thick-walled finite-length cylinders of functionally graded materials. J Thermal Stress 2005;28:391–408.
[42] Sager RJ, Klein PJ, Lagoudas DC, Zhang Q, Liu J, Dai L, et al. Effect of carbon nanotubes on the interfacial shear strength of T650 carbon fiber in an epoxy matrix. Compos Sci Technol 2009;69:898–904.
[43] Saito R, Dresselhaus G, Dresselhaus M. Physical properties of carbon nanotubes. London: Imperial College Press.; 1998.
[44] Salvetat-Delmotte J-P, Rubio A. Mechanical properties of carbon nanotubes: a fiber digest for beginners. Carbon 2002;40:1729–34.
[45] Sanchez-Palencia E. Non-homogeneous media and vibration theory. Lecture notes in physics, vol. 127. Springer-Verlag; 1978.
[46] Seidel GD. Micromechanics modeling of the multifunctional nature of carbon nanotube–polymer nanocomposites. Ph.D. thesis; 2007.
[47] Seidel GD, Lagoudas DC. Micromechanical analysis of the effective elastic properties of carbon nanotube reinforced composites. Mech Mater 2006;38:884–907.
[48] Spanos PD, Kontsos A. A multiscale Monte Carlo finite element method for determining mechanical properties of polymer nanocomposites. Probab Eng Mech 2008;23(4):456–70.
[49] Star A, Stoddart J, Steuerman D, Diehl M, Boukai A, Wong E. Preparation and properties of polymer-wrapped single-walled carbon nanotubes. Angew Chem Int Ed 2001;40(9):1721–5.
[50] Tarn J-Q. Exact solutions of a piezoelectric circular tube or bar under extension, torsion, pressuring, shearing, uniform electric loading and temperature change. Proc Roy Soc Lond 2002;458:2349–67.
[51] Tarn J-Q, Wang Y-M. Laminated composite tubes under extension, torsion, bending, shearing and pressuring: a state space approach. Int J Solids Struct 2001;38:9053–75.
[52] Thostenson ET, Li WZ, Wang DZ, Ren ZF, Chou TW. Carbon nanotube/carbon fiber hybrid multiscale composites. J Appl Phys 2002;91(9):6034–7.
[53] Tsukrov I, Drach B. Elastic deformation of composite cylinders with cylindrically orthotropic layers. Int J Solids Struct 2010;47:25–33.
[54] Tsukrov I, Drach B, Gross TS. Influence of anisotropy of pyrolytic carbon on effective properties of carbon/carbon composites. In: Proceedings of the seventeenth international conference on composite materials, Edinburgh (UK); 2009.
[55] Wagner H. Nanotube–polymer adhesion: a mechanics approach. Chem Phys Lett 2002;361(1–2):57–61.
[56] Wagner H, Lourie O, Feldman Y, Tenne R. Stress-induced fragmentation of multiwall carbon nanotubes in a polymer matrix. Appl Phys Lett 1998;72(2):188–90.
[57] Wang ZL, Gao RP, Poncharal P, de Heer WA, Dai ZR, Pan ZW. Mechanical and electrostatic properties of carbon nanotubes and nanowires. Mater Sci Eng C 2001;16:3–10.
[58] Yakobsona B, Smalley R. Fullerene nanotubes: C1,000,000 and beyond. Am Sci 1997;85 [review of nanotubes].
[59] Yakobson BI, Campbell MP, Brabec C, Bernholc J. High strain rate fracture and C-chain unraveling in carbon nanotubes. Comput Mater Sci 1997;8:341–8.
[60] Yamamoto N, Hart A, Garcia E, Wicks S, Duong H, Slocum A, et al. High-yield growth and morphology control of aligned carbon nanotubes on ceramic fibers for multifunctional enhancement of structural composites. Carbon 2009;47(3):551–60.
[61] Yu M-F, Files BS, Arepalli S, Ruoff R. Tensile loading of ropes of single wall carbon nanotubes and their mechanical properties. Phys Rev Lett 2000;84(24):5552–5.
[62] Zhao Z-G, Ci L-J, Cheng H-M, Bai J-B. The growth of multi-walled carbon nanotubes with different morphologies on carbon fibers. Carbon 2005;43(3):663–5.
[63] Zhu J, Kim J, Peng H, Margrave J, Khabashesku V, Barrera E. Improving the dispersion and integration of single-walled carbon nanotubes in epoxy composites through functionalization. Nano Lett 2003;3(8):1107–13.
[64] Zhu S, Su C, Lehoczky S, Muntele I, Ila D. Carbon nanotube growth on carbon fibers. Diamond Relat Mater 2003;34(12):1825–8.